Post-Mating Inhibition of Female Sexual Drive via Heterogeneous Neuronal Ensembles in the Medial Preoptic Area

Kentaro K Ishii[1,2], Koichi Hashikawa[1,2], Jane Chea[1,2], Shihan Yin[1,2], Rebecca Erin Fox[1,2], Suyang Kan[1,2], Charles Zhou[1,2], Jovana Navarrete[1,4], Alexandria D. Murry[1,4], Eric R Szelenyi[1,4], Sam A. Golden[1,4], Garret D. Stuber[1,2,3]

1. Center for the Neurobiology of Addiction, Pain, and Emotion, University of Washington, Seattle, WA, 98195, USA
2. Department of Anesthesiology and Pain Medicine, University of Washington, Seattle, WA, 98195, USA
3. Department of Pharmacology, University of Washington, Seattle, WA, 98195, USA
4. Department of Biological Structure, University of Washington, Seattle, WA, 98195, USA

Running title: Neural substrate for negative control of female sexual motivation

Highlights:

- **Female mice show decreased sexual motivation after mating completion.**
- **A subset of MPOA neurons respond specifically to mating completion.**
- **Mating completion evokes persistent activity in MPOA inhibitory neurons.**
- **Activation of a subset of MPOA neurons is sufficient to suppress female sexual motivation.**

SUMMARY

The completion of mating acutely suppresses sexual motivation in male mice. In contrast, relatively little is known about how the completion of mating affects sexual motivation and sexual behavior in female mice. How the brain responds to completion of mating is also unclear. Here, by using self-paced mating assay, we first demonstrate that female mice show decreased sexual motivation after the completion of mating. By using brain-wide analysis of activity-dependent labeling, we next pin-pointed the medial preoptic area as a brain region strongly responding to mating completion. Furthermore, using freely moving *in vivo* calcium imaging to compare neural activity of inhibitory and excitatory neurons in the medial preoptic area, we revealed that a subset of neurons responds significantly and specifically to mating completion but not to appetitive or consummatory behaviors. While there were excitatory and inhibitory neurons that showed positive response to the completion of mating, the response magnitude as well as the proportion of neurons responding to the event was significantly larger in the inhibitory neuron population. Next, by unbiased classification of their responses, we also found a subpopulation of neurons that increase their activity late after the onset of the completion of mating. These neurons were all inhibitory indicating that the completion of mating induces a prolonged inhibitory activity in the medial preoptic area. Lastly, we found that chemogenetic activation of medial preoptic area neurons that respond to mating completion, but not to appetitive behaviors, was sufficient to suppress female sexual motivation. Together, our data illuminate the importance of medial preoptic area as a brain node which encodes a negative signal that sustains low sexual motivation state after the completion of mating in female mice.

Introduction:

Sexual behavior is a fundamental and universal component of the observable behavioral spectrum in all mammalian species. This behavior results in reproduction, the vital process for species propagation. However, reproduction carries significant burdens, particularly for females, spanning pregnancy, birth, nursing, offspring rearing, and heightened vulnerability to environmental threats. Consequently, the female ability to strictly control sexual drive is adaptive and confers individual survivability. This can involve both increasing and decreasing motivation to engage in sexual behavior, dependent on anticipated beneficial outcome. Rodents provide a powerful resource for studying female sexual behavior and the underlying neural basis (Agrati, 2022; Micevych and Meisel, 2017). Typically, rodent sexual behavior is divided into three periods: an appetitive, consummatory, and post-copulatory phase (Hashikawa et al., 2016; Ishii and Touhara, 2018; Lenschow and Lima, 2020). The transition from the consummatory to the post-copulatory phase is triggered by the completion of mating, which is often associated with ejaculation from the male animal. Importantly, in males, sexual motivation acutely reduces after the completion of mating (Hull et al., 2005). However, less is known about how mating completion impacts female sexual behavior and motivation. Furthermore, how the transient experience of mating completion is represented in the brain to change the behavioral outcome is not well understood.

The medial preoptic area (MPOA), a molecularly and functionally heterogenous brain region, has classically been known to regulate wide variety of social behaviors (Fang et al., 2018; Hashikawa et al., 2021; Karigo et al., 2021; Kohl et al., 2018; Moffitt et al., 2018; Tsuneoka and Funato, 2021; Wei et al., 2018). Indeed, the MPOA has also been described to be an important brain area for the regulation of, including female sexual behavior. Studies in female rats using electrophysiological recording or histological approaches have reported that the MPOA contains neurons with various response specificity to sexual appetitive behaviors, consummatory behaviors and completion of mating (Kato and Sakuma, 2000; Pfaus et al., 1993). Similarly, MPOA lesions increased sexual receptivity, suggesting that the MPOA negatively regulates female sexual behavior when intact (Powers and Valenstein, 1972). Interestingly, the MPOA has also been found to positively regulate female sexual appetitive behavior through their projection to the mesolimbic reward system (McHenry et al., 2017). How the MPOA both positively and negatively regulate female sexual behavior, furthermore, sexual motivation, has been a long-lasting question in the field.

Here, we first assess sexual motivation in female mice by quantifying measurable approach or avoidance of a male conspecific. Next, by combining cellular-resolution whole-brain mapping of activity-dependent labeling, *in vivo* calcium imaging, and chemogenetic neural manipulation, we find that a subset of neurons in the MPOA, which are largely inhibitory, respond to mating completion but not to sexual appetitive behavior. This population is sufficient to suppress female sexual motivation. Our findings illuminate the importance of the MPOA as a brain region that encodes a negative signal that sustains low sexual motivation following the completion of mating in female mice.

Results:

Female sexual motivation is suppressed after mating completion.

Experimentally, sexual motivation can be quantified by the frequency of a subject displaying appetitive behavior, such as approach and sniffing behavior, toward an opposite sex conspecific. However, in a traditional rodent mating assay, where the female and male both freely interact with each other, it is difficult to isolate female-initiated appetitive behavior, and thus their sexual motivation. To directly address aspects of female sexual motivation independent from the male's behavior, we used a female self-paced mating assay (Erskine, 1989; Peirce and Nuttall, 1961). In this procedure, a female subject and a sexually experienced male are placed in a behavior

apparatus divided by a wall with a hole small enough for a female to move through, but not the male. The female subject may move into the room where the male animal was placed ("Interaction zone") or move out to the other room ("Isolation zone") (**Figure 1A**). Thus, in this assay the female has direct control of when interaction happens and provides a more ethologically valid measure of female appetitive sexual behavior. Specifically, the amount of time the female subject spends in the interaction zone and the number of transitions they make serve as metrics to quantify female appetitive behavior. On the experiment day, the female subject was placed in the apparatus with the male intruder ("Sexual interaction" trial) or alone ("Control" trial). Each animal went through both trials on different experiment days. The position of the animal was tracked to quantify the time spent in each zone. First, we found that the virgin female mice stayed in the isolation zone significantly longer than sexually experienced females, suggesting that previous sexual experience increased sexual motivation in the female mice (**Figure S1**). Next, in the sexually experienced animals, we observed robust behavioral changes after the completion of mating (**Figure 1B**). First, we observed that female subjects tended to spend more time in the isolation zone after mating completion compared to post- sniffing, mounting and intromission (**Figure 1C–F**). To quantify the changes in animal behavior, we divided the sexual interaction trial into pre- and post- mating completion epochs (**Figure 1G–I**). As result, we found that there was a significant decrease in the number of zone transitions as well as a significant increase in the time spent in the isolation zone after the completion of mating. In addition, while there was no change in the amount of female-to-male sniffing, there was a significant decrease in the number of mounting and intromission episodes (**Figure 1J–L**). There was also a significant increase in the number of self-grooming behavioral episodes (**Figure 1M**). Collectively, these results suggest that the completion of mating decreases sexual motivation.

Brain-wide mapping of neural response to mating completion using activity-dependent labeling in the female brain.

We next questioned how mating completion suppresses female sexual motivation. To investigate this question, we first determined which brain regions were associated with neural activity following the completion of mating in an unbiased manner. We conducted a cellular-resolution brain wide activity mapping analysis using targeted recombination in active populations method (TRAP), which allows genetic labeling and access to neurons that are active during a specific time window determined by tamoxifen administration (DeNardo et al., 2019). To capture the activity pattern associated with mating completion, Fos-2A-iCreER^{T2}::RCL-tdTomato (TRAP2::Ai14) female mice were administered 4-hydroxytamoxifen (4-OHT) immediately after the completion of mating ("Completion" group) (**Figure 2A**). In this method, cells that show behaviorally induced Fos activity were labeled with tdTomato. In addition to these animals, we also prepared a group of animals that were administrated with 4-OHT while the animals were in the appetitive phase. Female subjects interacted with male mice but did not experience any mount or intromission behavior, nor did it complete mating ("Appetitive" group). After 2 weeks, the tissue was collected, cleared, imaged, and processed for registration on a template brain atlas (Park et al., 2019; Renier et al., 2016) (**Figure 2A**). The tdTomato+ cells were segmented using a trained classifier and normalized by the area of each brain region (**Figure 2B**). As result, we found mating completion increased tdTomato expression a brain wide manner (**Figure 2C–D**, **Table 2**). We further noticed that regions well known to be related to social behavior had significantly higher tdTomato density in the Completion group compared to the Appetitive group (**Figure 2E–I, Figure S2, Table 3**). This includes paraventricular hypothalamic areas (PVHd, PVH, PaV) which are important for endocrinological regulations, medial amygdala (MeA) which is critical for olfactory sensory information processing, and the BNST (Flanigan and Kash, 2022; Marsh et al., 2021; Raam and Hong, 2021). The medial preoptic area nucleus (MPN), a subregion of the MPOA, had significantly higher tdTomato density in the Completion group compared to the Appetitive group. The MPN

also had the 4th largest difference of density between Completion group and Appetitive group among all the brain regions. From this result, we decided to further investigate the role of MPOA and how it is related to the regulation of female sexual motivation after the completion of mating.

Mating completion is represented by both inhibitory and excitatory cell types in the MPOA. MPOA is a molecularly heterogenous brain region. The area is a mixture of 80% inhibitory neurons and 20% of excitatory neurons which can be further classified into neuronal subtypes by marker gene expressions (Hashikawa et al., 2021; Moffitt et al., 2018). These subtypes are often associated with a biological function. One example are the *Nts* expressing cells, which also tend to co-express *Esr1* and *Vgat* (McHenry et al., 2017). In female mice, these neurons were shown to respond to male odor when the subject was sexually receptive, and the activation of these neurons were sufficient to increase sexual appetitive behaviors. Therefore, identifying the specific cell types which respond to mating completion but not to appetitive behavior is critical to understand how the MPOA complex regulates female sexual motivation. Here, we utilized multiplexed *in situ* RNA hybridization chain reaction (HCR) to identify previously characterized cell type markers of MPOA and an immediate early gene *Fos* (**Figure S3A**) (Choi et al., 2014). Brain samples were collected after the completion of mating ("Completion" group) or during the appetitive phase; while the subject was interacting with the male mice without any consummatory behavior ("Appetitive" group) (**Figure S3B**). First, to understand which subregion of the preoptic area was activated, we quantified the number of *Fos*+ cells. As result, we found that the number of *Fos*+ cells in the Completion group were significantly higher than the Appetitive group in the MPN but not in the nearby regions (**Figure S3C–D**). In the MPN, the amount of *Vglut2*+ and *Vgat*+ cells expressing *Fos* were significantly higher in the Completion group than in the Appetitive group, suggesting that the completion of mating activates both excitatory and inhibitory neurons (**Figure S3E–I**). The proportion of *Fos*+ cells was higher in *Vgat*+ population. To further investigate the cell types in the MPN that were activated by mating completion, we analyzed the co-expression of *Fos* and the MPOA cell type markers (**Figure S3J**). As result, in the *Vglut2*+ expressing cells, we found that *Fos* induction was only observed in the cells that co-expressed *Calcr*. In contrast, in the *Vgat*+ expressing cells, *Fos* induction was observed in *Calcr, Gal* and *Prlr* co-expressing cells. Next, we conducted clustering on the gene expression matrix to classify cells and analyzed the distribution of *Fos* among the clusters (**Figure S3K–M**). As result, we were able to identify 6 potential cell types which we labeled as type 1: *Vglut2*+, type 2: *Vgat*+, type 3: *Gal*+, type 4: *Nts*+, type 5: *Calcr*+ and type 6: NA, or a cell group that could not be categorized by a specific gene expression pattern. Type 1: *Vglut2*+, type 2: *Vgat*+ and type 3: *Gal*+ had significantly more *Fos*+ cells from the Completion group compared to the Appetitive group (**Figure S3M**). In contrast, *Fos*+ cells were not induced in type 4: *Nts*+ indicating that MPOA neurons which regulate appetitive sexual behavior was not activated by mating completion. Collectively, these results indicate that mating completion induces more neural activity in the MPN when compared to appetitive behavior, both in excitatory and inhibitory cell types.

A subpopulation of MPOA Vgat cells respond to mating completion in the female brain. While mapping neural activity based on Fos activity provided critical insight in how the brain responds to mating completion, the low temporal resolution of the method makes it difficult to identify cells that specifically respond to the onset to each behavior. For this reason, we next conducted single-cell resolution *in vivo* imaging in a freely moving animal (**Figure 3A–B**). We virally labeled MPOA inhibitory and excitatory cells with a calcium indicator GCaMP6s by using a Cre-dependent virus and female Vgat-Cre or Vglut2-Cre respectively **(Figure 3C, Figure S4**) (Vgat-Cre: n = 6, 87 ± 27 cells. Vglut2-Cre: n = 4, 68 ± 42 cells). We recorded the calcium activity of MPOA Vgat and Vglut2 cells in female mice during mating in a home cage mating assay (**Figure 3E**). First, we analyzed the magnitude of calcium activity for 15-seconds after behavior

onset. From peri-event analysis, we found that as a population, Vgat cells showed significant changes in calcium activity after the onset of all behaviors observed, with the highest increase after mating completion (**Figure 3F–G**). Vglut2 cells showed increased activity after sniffing and mounting, intromission, and mating completion. Furthermore, when we compared the response of Vgat and Vglut2 cells, Vgat cells showed significantly higher average response magnitude after sniffing, self-grooming, anogenital sniffing and mating completion than the Vglut2 cells (**Figure 3H**). Vgat cells also contained a significantly higher proportion of cells that positively respond (> 2δ) to sniff and mating completion onset (**Figure 3I**). These results suggest that mating completion signal is more dominantly represented in the MPOA inhibitory cells than in the excitatory cells. On the other hand, the response magnitude and the proportion of cells that respond after mounting and intromission had no significant difference between the two cell types. This indicates that the excitatory/inhibitory balance in the MPOA fluctuates during mating. The MPOA has high inhibitory activity during appetitive phase, with more Vgat cells responding to sniffing, similar activity during the consummatory phase, and higher inhibitory activity after mating completion.

To further investigate the heterogeneity of MPOA during mating, we subset the cells into those which positively responded to any of sniff, mount or mating completion, and then classified the cells based on their specificity (**Figure 4A,B** and **Figure S5**). Consistent with **Figure 3I**, the number of cells that specifically responded was largest to mating completion with 177 cells, next to mount with 46 cells and to sniff with 12 cells. When compared to other cell populations, sniff cells and completion cells only showed significantly stronger responses than the other cells to sniff and mating completion respectively (**Figure 4C**). Mount responsive cells showed significantly stronger response than the other cells to mount, intromission and anogenital sniffing, but not to sniffing and mating completion (**Figure 4C**). We also found that the cells that respond to these 3 behaviors partially overlap but were mostly distinct (**Figure 4D**). The proportion of cells that respond specifically to a behavior was highest for mating completion (Vgat: 80%, Vglut2: 82%), and lower in mounting (Vgat: 55%, Vglut2: 68%) and sniffing (Vgat: 36%, Vglut2: 0%). There was no notable bias in the anatomical distribution of these cells within the field of view (**Figure 4E**). Overall, these results suggest that the MPOA contains highly heterogenous functional population which contains a large proportion of cells specifically responding to mating completion in female mice.

MPOA Vgat cells display prolonged activity after the onset of mating completion.

Female mice avoid sexual interaction with a male animal after mating completion for hours and even days, suggesting a persistent changes in the animal's behavior (McGill and Coughlin, 1970; Zhou et al., 2023). How the MPOA regulate this persistent change in female sexual motivation is unclear. To analyze the response of MPOA cells on a longer time scale, we focused on the cells that positively responded to mating completion and characterized the calcium response pattern for 120-seconds after the onset (**Figure 5**). First, we observed that Vgat cells showed more diverse response patterns during this time-window (**Figure 5A,B**). To quantify this difference, we calculated the decay length of calcium signal, the time for the increased calcium signal to return to baseline (**Figure 5C**). As result, we found that Vgat cells had significantly longer decay length compared to the Vglut2 cells, suggesting increased activity late after the onset of the completion of mating. To further classify the temporal dynamics of responses to mating completion, we first concatenated calcium activity that occurred within this time-window from both Vgat and Vglut2 cells and conducted spectral clustering in an unbiased fashion. As result, we were able to classify the responses into 5 types that could be characterized as: 1) fast response, 2) slow response, 3) late response, 4) weak response and 5) negative response (**Figure 5E**). Type 3 contained cells that show increased calcium dynamics late after the onset of mating completion and had significantly larger decay length than the other cell types (**Figure 5F**). Then we separated the Vgat and Vglut2 cells to compare their proportions within each cluster. Interestingly, all the cells

in type 3 were Vgat cells, suggesting that the increased activity in the MPOA late after the onset of mating completion is mediated by inhibitory neurons (**Figure 5H–K**). In contrast, Vglut2 cells were more likely to show fast responses than Vgat cells (**Figure 5K**). Collectively, these results suggest that the MPOA contains a subpopulation of inhibitory neurons which increase their activity late after the onset of mating completion, which may contribute to persistent suppression of the female animals' sexual motivation.

An activity defined subset of neurons in the MPOA is sufficient to suppress female sexual behavior.

Next, we examined whether the increased activity of neurons in the MPOA is sufficient to suppress female sexual motivation after mating completion. We injected an AAV to express the chemogenetic neural activator hM3Dq or eYFP as control into the MPOA of TRAP2 female mice (**Figure 6A**). To capture the neural activity, each mouse was administrated 4-OHT immediately after the after the completion of mating ("Completion-hM3Dq" or "Completion-eYFP" group). In addition to these animals, we also prepared a group of animals in which we injected an AAV expressing hM3Dq and then administrated 4-OHT during the appetitive phase ("Appetitive-hM3Dq" group) (**Figure 6C**). We found that while the overall number of TRAP-labeled cells had no difference between the Completion groups and the Appetitive group, the proportion of cells located in the MPN was significantly higher in the Completion groups (**Figure 6D** and **Figure S7A–D**). From *in situ* RNA hybridization, we found that most TRAP-labeled cells in the MPN were *Vgat*+ (*Vgat*+: 0.76 ± 0.16. *Vglut2*+: 0.15 ± 0.13.). The proportion of *Vgat*+ cells was significantly higher than the *Vglut2*+ cells (**Figure S7E–H**). Together these results suggest that the Completion group labels more inhibitory neurons in the MPN than in the Appetitive group. Furthermore, we analyzed the accuracy and efficiency of TRAP labeling by exposing the animal to mating completion before perfusing the animal. By labeling c-Fos protein signal, we analyzed how well the TRAP ensemble overlaps with the c-Fos positive-ensemble in the MPN. As result, we first found that the number of TRAP-labeled cells as well as c-Fos+ and TRAP-labeled cells in the Completion group was higher than the Appetitive group, consistent with the previous results (**Figure S7J, 6K**). Next, we found that the accuracy of TRAP labeling (the proportion of TRAP-labeled cells that were also c-Fos positive) was similar between the groups (**Figure S7J**, Completion group 0.44 ± 0.08, Appetitive group 0.51 ± 0.31). The efficiency of TRAP labeling (the proportion of c-Fos+ cells that were also TRAP labeled) tended to be higher in the Completion group (**Figure S7J;** 0.12 ± 0.10) than in the Appetitive group (0.03 ± 0.02). This also suggests that the Appetitive group labels a different set of neurons than the Completion group. These results indicate that by using the TRAP2 method, we were able to specifically label a proportion of MPOA neurons, which are primarily inhibitory, that respond specifically to mating completion.

To test the causality of these neurons, we first investigated how the activation affects female sexual behavior in a home cage mating assay (**Figure S8A–F**). The subjects were intraperitoneal injection (i.p.) injected with CNO 30-minutes before the assay. As result, first we found that Completion-hM3Dq groups showed significantly fewer sniffing events compared to Completion-eYFP and Appetitive-hM3Dq groups (**Figure S8C**). For consummatory behaviors, while Completion-hM3Dq group showed no difference in mounting episodes compared to Completion-eYFP and Appetitive-hM3Dq groups, there were significantly less intromission episodes, resulting in lower receptive scores (**Figure S8D–F**). Thus, from these results, activation of MPOA neurons that respond to mating completion suppresses both appetitive and consummatory sexual behavior in female mice.

As a next step, we investigated how the activation of these MPOA neurons affects female sexual motivation in a self-paced mating assay (**Figure 6**). The subjects were i.p. injected with CNO or saline 30-minutes before the assay (**Figure 6B**). As result, Completion-hM3Dq group, but not Completion-eYFP and Appetitive-hM3Dq group, showed significantly fewer number of

transitions and spent more time in the isolation zone on the CNO trial than on the saline trial (**Figure 6E–G**). We also found that Completion-hM3Dq group, but not Completion-eYFP and Appetitive-hM3Dq group, displayed fewer numbers of self-grooming, mounting, intromission and lower receptivity score on the CNO trial than on the saline trial (**Figure 6H–L**). Interestingly, activation of these neurons did not induce conditional place preference or aversion (**Figure S8G–J**), implying that the suppression of sexual behavior is not associated with negative valence. Collectively, these results suggest that the activation of a subset of inhibitory neurons in the MPOA that respond to mating completion is sufficient for the suppression of female sexual motivation (**Figure 6M**).

Discussion:

How sexual motivation is represented in the brain has been a long-lasting question in the field. Here we found that MPOA plays a critical role in regulating female sexual motivation. We found that MPOA neurons, especially the inhibitory neurons, respond significantly and specifically to the completion of mating. These neurons show persistent activity after the onset of mating completion. Reactivation of these neurons result in suppression of female sexual motivation. We propose that MPOA together with other neural substrates such as the BNST (Zhou et al., 2023), encode a negative feedback signal that sustains low sexual motivation state after the completion of mating in female mice. Here, we will further discuss how sensory inputs contribute to the mating completion response in the MPOA, how MPOA represents appetitive behavior and mating completion signal and how these neurons work in concert with other sexual behavior related hypothalamic regions.

Sensory representation of mating completion in the female brain and genitalia.

Suppression of female sexual behavior and motivation after the completion of mating is not a unique phenomenon found in mice and can be observed in various insect species (Gillott, 2003). Studies in *Drosophila* has demonstrated that the primary trigger of this behavioral switch is the sex peptide (SP), a peptide released in the male seminal fluid (Chapman et al., 2003; Chen et al., 1988; Liu and Kubli, 2003). Studies in flies have further identified the receptor for SP as well as the neural circuitry which conveys the sensory information to the mating regulating neurons in the brain (Feng et al., 2014; Rezával et al., 2012; Yapici et al., 2008). In contrast to the well-studied system in *Drosophila*, little is known about how the mammalian brain senses the completion of mating. Histological studies in rats have shown that mating completion induces c-Fos expression widely in the brain, including the MPOA (Pfaus et al., 1993). Indeed, anesthesia to the female genitalia has been shown to disrupt pacing of mating, indicating that sensory input from the genitalia can impact female sexual behavior (Parada et al., 2014). Furthermore, artificial stimulation of the vagina or the clitoris of the female rat was further shown to induce c-Fos expression in the MPOA in a similar fashion as mating completion, indicating that at least tactile sensory input can be conveyed to this brain area (Parada et al., 2010; Pfaus et al., 1996). Ejaculation from vasectomized male animals were sufficient to suppress sexual behavior suggesting that at least chemical components from the testis is not necessary for this effect (Zhou et al., 2023). A recent study has shown that mechanical stretch induces serotonergic activity in the dorsal raphe, which resembles changes after mating completion, suggesting that stretch sensation is mediating mating completion signal to the brain (Troconis et al., 2023). However, it is unclear how stretch sensation in the genitalia is conveyed to the brain, and equally unclear how this information is ultimately transmitted to the MPOA. Our findings on how the mating completion

signal is represented in the MPOA will be an ideal entry point to study the neural basis of genital-brain communication.

Appetitive behavior and mating completion ensembles in MPOA.

The MPOA is a molecularly and functionally heterogenous brain region. One function MPOA has heavily been related to is parenting behavior. MPOA neurons which express *Gal* and/or *Calcr* has been demonstrated to regulate parenting behavior (Kohl et al., 2018; Wu et al., 2014; Yoshihara et al., 2021). From our data, neurons that respond to mating completion tended to co-express *Gal* and *Calcr* more than neurons that responded to appetitive behavior (**Figure S3**). However, we also found that chemogenetic activation of mating completion responsive MPOA neurons did not induce parenting behavior (**Figure S8**). While it is necessary to conduct extensive analysis of how MPOA neurons respond to other behaviors, these results suggest that mating completion responding MPOA neurons may specifically regulate sexual behavior and motivation but not parenting behavior. A previous study also found that MPOA contains a subset of neurons which regulate female appetitive sexual behavior. MPOA neurons which express *Vgat, Esr1* and *Nts*, and projects to the ventral tegmental area (VTA) has been shown to respond to olfactory signals from the male mouse and to enhance female-to-male sniffing (McHenry et al., 2017). There is also a significant release of dopamine after the first female to male sniffing interaction as well as after mating completion (Dai et al., 2022). How the brain, especially the MPOA, increases sexual motivation before and during the appetitive phase, and how it suppresses motivation after the completion of mating, has been a long-lasting question in the field that is addressed throughout this work. The whole brain activity-dependent labeling experiment identified the MPOA as one of the brain regions which strongly increases Fos activity (**Figure 2**).

However, there were many other brain regions showing increased activity associated with mating completion, including ones that are not canonically involved in the regulation of social behavior. While it is possible that all these brain regions work in concert to suppress sexual motivation after the completion of mating, our results demonstrate that a specific brain region, MPOA, is sufficient to evoke behavioral response. This suggests that all brain regions showing higher Fos activity are not necessarily causal to behavioral changes. It is also possible that these widespread brain regions may be a consequence of noise due to the long time-window in this method, which may be resolved by further development of genetic methods for neural ensemble labeling. In the MPOA, our *in vivo* calcium imaging data shows nearly half of the inhibitory neurons that positively respond to appetitive behavior also respond to mating completion (**Figure 4**). Our data also identified that there was no difference between the number of *Nts*+ cells activated by appetitive behavior and mating completion (**Figure S3**). These results suggest that there is a small but significant number of neurons which respond both to appetitive behavior and mating completion in the MPOA, and potentially regulate release of dopamine.

Although a large amount of appetitive behavior responding neurons also respond to mating completion, the opposite is not true. Most of the mating completion responding neurons did not respond to female-to-male sniffing (**Figure 4**). Importantly, the chemogenetic activation of this population suppressed the amount of sexual interaction in the self-paced mating assay, which suggest that it reduces sexual motivation, opposite to what was described when activating *Nts*+ MPOA neurons (McHenry et al., 2017). This suggests that there are at least two-distinct populations in the MPOA which regulate appetitive sexual behavior in opposing directions.

Neural circuitry for female sexual behavior regulation:

The neural circuitry that regulates female sexual behavior has been extensively studied in rodent models. From early lesion and electrical stimulation studies, it has been proposed that the rodent brain has a positive and negative regulatory system for female sexual behavior. The positive system has been proposed in rats, where Pfaff and Sakuma demonstrated that the lesion of the

ventromedial hypothalamus (VMH) abolished sexual receptivity while electrical stimulation of the same region induces receptivity (Pfaff and Sakuma, 1979a, 1979b). Mouse genetics further showed that a subset of neurons in the ventrolateral part of the VMH is crucial for the regulation of female sexual behavior (Inoue et al., 2019; Yang et al., 2013). More specifically, *Esr1*+ *Cckar*+ (*Nts*-) cells in the VMHvl were found to be necessary and sufficient for female sexual receptivity (Liu et al., 2022; Yin et al., 2022). These results suggest that the VMHvl is the "command center" which positively regulate female sexual behavior.

The MPOA together with other brain regions has been proposed to form the negative regulating system. Lesion of the MPOA was shown to increase the sexual receptivity of the female rat and electrical stimulation was shown to reduce receptivity, suggesting that MPOA negatively regulates female sexual behavior (Pfaff and Sakuma, 1979b; Powers and Valenstein, 1972). In the current study, we demonstrate that chemogenetic activation of neurons in the MPOA which respond to mating completion is sufficient to suppress female sexual behavior and sexual motivation. This result suggests that these neurons in the MPOA constitute the negative regulating system. Importantly, both our single-cell calcium imaging results and histological analysis of the chemogenetic activation cohort suggest that the majority of these neurons are inhibitory (**Figure 3I** and **Figure S7H**). We further demonstrate that the inhibitory population contains neurons that show prolonged responses to mating completion which resemble the persistent change of sexual motivation. Other studies have also supported the idea that the inhibitory cell population is more related to the regulation of social behavior than the excitatory population (Fang et al., 2018; Hashikawa et al., 2021; Moffitt et al., 2018; Tsuneoka and Funato, 2021; G.-W. Zhang et al., 2021). Our results are also in line with this idea and suggest that the inhibitory neuronal population is the main regulator of the change in sexual motivation. The role of excitatory neurons that respond to mating completion will be a future topic to examine.

Recently, BNST was also found to play a role in negatively controlling female sexual behavior (Zhou et al., 2023). There, they use a behavioral assay which introduces 2 different males to the female subject before and after the completion of mating. They demonstrate that after the completion of mating, the female will be less receptive toward the second male. Importantly, this assay clearly demonstrate that the reduction of female sexual behavior is due to the female herself, not due to the change in their male conspecific. This result together with the result from our self-paced mating assay (**Figure 1**) strongly indicates that the behavioral change after mating completion reflects change in internal motivational states.

The study further used single-cell resolution *in vivo* calcium imaging techniques to demonstrate that $BNST^{Esr2}$ neurons show specific and robust responses after mating completion, like what we observed in the MPOA. While inhibition of $BNST^{Esr2}$ neurons rescued female receptivity after mating completion, activation of these neurons did not affect sexual behavior in female mice, suggesting that $BNST^{Esr2}$ neurons are necessary but not sufficient to suppress female sexual behavior or potentially sexual motivation. This result may suggest that $BNST^{Esr2}$ neurons require activation of other neural populations to affect female sexual behavior, such as the populations we identify in the MPOA. Still, the overall role of BNST and MPOA seems to be similar suggesting that the two regions work in concert to suppress female sexual behavior. This is contrary to the finding from Mei et al. showing that the $BNST^{Esr1}$ neurons and $MPOA^{Esr1}$ neurons forms a bidirectional inhibitory circuit to antagonistically regulate infanticidal behavior and maternal behavior respectively (Mei et al., 2023). A mechanism which is yet to be revealed that can override the negative feedback loop between MPOA and BNST neurons is necessary for these neurons to regulate the same behavior change. Interestingly, (Yin et al., 2022) showed that $VMHvl^{Cckar}$ neurons show strong inhibition of spontaneous bulk calcium events after mating completion (Yin et al., 2022). This is opposite to the persistent increase of activity in the MPOA and BNST, suggesting that the activity in these regions is reflected onto the VMHvl. Indeed, MPOA and BNST both send dense projection to the VMHvl, and $VMHvl^{Esr1}$ neurons project to the

MPOA and to the BNST, making the MPOA-BNST-VMHvl network highly interconnected (Dimén et al., 2021; Lo et al., 2019; Osakada et al., 2018).

Long-lasting change in neural activity within this network, potentially through monoamine or steroid molecules such as dopamine or opioids may be the neural basis of suppressed sexual motivation after mating completion (Micevych and Meisel, 2017; S. X. Zhang et al., 2021). Another candidate is serotonin, which is known to be an important mediator for sexual behavior (Uphouse, 2014). Recent study has revealed release of serotonin in response to mating completion in female mice (Troconis et al., 2023). Our whole brain activity mapping data also indicates increased Fos activity in the dorsal raphe (**Figure S2**). Whether serotonin mediates the changes in persistent activity across the entire network and whether there is a difference in how it impacts MPOA and BNST will be an important topic of future studies.

Taken together, our study identifies a subset of neurons in the MPOA which is dedicated to negatively sustain female sexual motivation. This finding fills the missing hole in how the brain neurons regulate female sexual motivation and proposes that the basal forebrain complex of MPOA and BNST work in concert as the negative regulating system of female sexual behavior.

Materials and methods:

Animals.

All experiments were approved by the Institutional Animals Care and Use Committee at the University of Washington (Protocol #4450-01). Animals were group-housed with littermates on a 12-hr light cycle at ~22°C with food and water available *ad libitum*. Wild-type Swiss-Webster mice were purchased from Taconic Biosciences (NY, U.S.). Wild-type C57BL/6 mice were purchased from the Jackson laboratory and bred in-house. Vgat-Cre (also known as *Slc32a1*-ires-Cre, Jax#016962), Vglut2-Cre (also known as *Slc17a6*-ires-Cre, Jax#028863) and Ai14 (Rosa-CAG-LSL-tdTomato-WPRE, Jax#007914) were purchased from Jackson laboratory. TRAP2 mice (also known as Fos-2A-iCreER^{T2}, (DeNardo et al., 2019)) were provided by Dr. Palmiter (University of Washington) and crossed with Ai14 to generate TRAP2::Ai14 mice. All male mice which were used as intruders were singly housed to avoid male-male aggression. Female mice with GRIN-lens implant were singly housed. All other mice were group housed.

Surgery.

For targeting AAV into a certain brain region, stereotactic coordinates were defined for each brain region based on the brain atlas (Franklin and Paxinos, 2007). Mice were anesthetized isoflurane and head-fixed to stereotactic equipment (Kopf). For *in vivo* calcium imaging experiments, 500 nL of AAVDj EF1a-DIO-GCaMP6s (2.8*e12, UNC viral core, lot#av78310) was injected into two coordinates in the target brain region at a speed of 60 nl/min using Nanoject 3 pump (Drummond Scientific). The following coordinates were used [Distance in millimeters from the Bregma for the anterior (A)-posterior (P) and lateral (L) positions, and from the brain surface for ventral (V) direction]: MPOA, A 0.2, L 0.15, V 5.2. and A 0.4, L 0.35, V 5.2. Immediately following viral injection, 5 screws were placed into the skull and a GRIN lens (Inscopix, 0.6 mm x 7.3 mm) was slowly lowered to position above the injection site: MPOA, A 0.3, L 0.3, V 4.95. GRIN lens was glued to the skull with C&B Metabond Kit (Parkell, # S380) and dental cement (Lang Dental, #1304CL). After placement of GRIN lens, a custom-made head ring was glued to the skull and screws. For bare GRIN lenses, more than 3 weeks after the virus injection and GRIN lens placement surgery, a baseplate (Inscopix) was positioned to while visualizing GCaMP6s expression with a microscope. Once a field of view with GCaMP6s expression was found, the baseplate was glued to the head ring and skull. For pharmacogenetic experiments, 300-400 nL of AAV5 hSyn-DIO-hM3D(Gq)-mCherry (2.0*e13, Addgene, #44361-AAV5, lot#v141469) or AAV5 EF1a-DIO-eYFP (4.4*e12, UNC viral core, lot#av4802B) was bilaterally injected into the target brain region at a speed of 60 nl/min using Nanoject 3 pump. The following coordinates were used: MPOA, A 0.3, L 0.25, V 5.2. All female mice that experienced a mating assay was ovariectomized. Animals that were used in *in vivo* calcium imaging experiments or pharmacogenetic experiments were ovariectomized during the virus injection or GRIN lens placement surgery. After surgery, the incision was sutured, and the animal was warmed using a heat pad to facilitate recovery from anesthesia.

Behavior experiments and analysis.

For all mating assays, female mice older than 6 weeks were ovariectomized (OVX) under isoflurane anesthesia. If necessary, mice underwent surgeries for AAV injections, GRIN lens implantation on the same day. After more than 2 weeks of recovery, the OVX female subjects were subcutaneously (s.c.) injected with 0.1 mL and 0.05 mL Estradiol (E8515, Sigma-Aldrich, 0.1 mg/ml) dissolved in sesame oil (Sigma-Aldrich) at 24 and 48h before assay, and 0.05 mL Progesterone (P0130, Sigma-Aldrich, 10 mg/ml in sesame oil) at 4h before assay. If necessary, mice underwent I.P. injection of CNO/saline. C57BL/6 or Swiss-Webster mice were used as a stud male. A 4 – 6 cm to head bar was placed onto the male mice under isoflurane anesthesia, which was used for the female self-paced mating assay described below. The male animals were

kept isolated until the assay and had been trained prior to the assay to show mounting and ejaculation.

The home cage mating assay was conducted as previously described with modifications (Ishii et al., 2017). Each assay was conducted 5-10 hrs after the onset of dark period, under an IR light and recorded (30 Hz) for subsequent 30 to 120 min for analysis of sexual behavior from a dorsal view. For neural activation experiments using hM3Dq (**Figure S5, Figure S6**), 0.1 mL of 1 mg/kg clozapine-N-oxide dissolved in saline (CNO, RTI International, NIMH Code C-929) or 0.1 mL of saline was I.P. injected into the animal 30 minutes prior to the male entry.

The female self-paced mating assay was conducted using a behavior apparatus modified from an apparatus used in rat (Nyuyki et al., 2011). A 1-cm thick black wall with a 20 mm x 20 mm hole 3D-printed with PFA filament was placed in a 25 cm x 35 cm cage to divide the room in a 1:2 ratio along the longer edge. The smaller room was defined as the isolation zone and the larger room was defined as the interaction zone. Female subjects were habituated to the room for 30 minutes before the assay. The female subjects that were not able to pass through the hole during the habituation was eliminated from the cohort. On the experiment day, the female subjects were placed into the behavior apparatus for 30 minutes for analysis of movement tracking from a dorsal view, which was used as control (Control trial). After the habituation, the male intruder (Swiss-Webster) was placed in the interaction zone. Each assay was conducted 5-10 hrs after the onset of dark period, under an IR light and recorded (15 Hz) for subsequent 30 to 120 min for analysis of movement tracking and sexual behavior from a dorsal view (Sexual interaction trial). For **Figure 6**, females underwent two mating assays at > 1 week interval, with different treatment (e.g., saline or CNO). Different males were used for each assay. For neural activation experiments using hM3Dq (**Figure 6, Figure S5, Figure S6**), 0.1 mL of 1 mg/kg clozapine-N-oxide dissolved in saline (CNO, RTI International, NIMH Code C-929) or 0.1 mL of saline was I.P. injected into the animal 30 minutes prior to the male entry.

Sexual behavior was annotated from the recorded video using Behavioral Observation Research Interactive Software (BORIS) in a frame-by-frame fashion (Friard and Gamba, 2016). Male mounts, intromission, male to female anogenital sniffing, female to male sniffing, female self-grooming and mating completion were annotated based on characteristic postures described previously (Ishii et al., 2017). Briefly, mount was defined as a stud male using both forepaws to climb onto a female from behind for copulation. Intromission was defined by stable thrusting from the male animal during mount. The completion of mating was identified by increase and then termination of thrusting and more than 10 seconds of immobility from the male, which are postures frequently associated with male ejaculation. Male to female anogenital sniffing was identified by the male animal following the female subjects anogenital area. Female to male sniffing was identified by female subject nose approaching male subject. When analyzing sniff-evoked GCaMP activity, to restrict the analysis to appetitive sniffing behaviors, sniffing behaviors which happened after the first mounting was excluded from the analysis. Female self-grooming was identified by the female subject moving their head close to their genital region. The receptive ratio was calculated by dividing the total number of intromissions with the total number of mountings. Behavior annotation was conducted by volunteers who were blind for the stimulation or AAV condition. For the female self-paced mating assay, the position of the female subject was tracked from the recorded video using DeepLabCut (Nath et al., 2019). The amount of time spent in the interaction zone was quantified using SimBA region of interest (ROI) interface (Nilson et al., 2020). Behavior data from *in vivo* calcium imaging experiments were down-sampled to 10-Hz to match the imaging data.

For conditional place preference (**Figure S8G–J**), a two chambered apparatus was used with visual (horizontal and vertical stripes) cues. The floor was backlit and an overhead video camera recorded position (Basler, 3.75 Hz frame rate with Ethovision software, Noldus). The apparatus was in a sound isolation chamber. *Ad libitum* fed Fos-CreER mice with hM3Dq and eYFP controls were acclimatized (60 min). The following day, the mouse's position was recorded

(1,800 s) and tracked offline using Ethovision (pre-test). Daily conditioning consisted of two 1,800 s sessions: (1) one side of the chamber paired with saline injection; (2) the other side paired with CNO (1 mg/kg) injection. Saline or CNO was administrated 10 min prior to the entry to the chamber. The side on which saline or CNO was administered was counterbalanced. After three conditioning days, mice were given free access to the entire apparatus and their position was tracked (post-test). The difference of time spent in the CNO zone, the number of entries into the CNO zone and the velocity between the post- and pre- test.

For pup retrieval test (**Figure S8K–O**), a home cage of the female subject was used. Female subject was i.p. injected with saline as control or CNO in their home cage. 30-minutes after administration, three 7-day-old pups were placed in the corners of the home cage. Animal behavior was recorded from the dorsal view for 10 minutes. Parenting behavior was annotated from the recorded video using Behavioral Observation Research Interactive Software (BORIS) in a frame-by-frame fashion. Pup retrievals, nest building, pup grooming and pup sniffing were annotated based on characteristic postures. Briefly, pup retrieval was defined as a female subject carrying pup. Nest building was defined by female subject digging their bedding or carrying nesting material. Pup grooming was identified by grooming pups without carrying. Female to pup sniffing was identified by female subject nose approaching pup. For neural activation experiments using hM3Dq (**Figure S6**), 0.1 mL of 1 mg/kg clozapine-N-oxide dissolved in saline (CNO, RTI International, NIMH Code C-929) or 0.1 mL of saline was I.P. injected into the animal 30 minutes prior to the pup introduction.

***In vivo* calcium imaging experiments and analysis.**

Miniature microscope nVoke 2.0 or nVue (Inscopix) was used to obtain GCaMP6s signal (20 Hz). The microscope was connected above the behavior apparatus using a commutator (Inscopix) to support the weight of the microscope. On the experiment day, the subject was habituated to the microscope for 10 minutes. After the habituation, the LED power and gain was adjusted to 0.2-0.5 and 6.0-8.0 respectively depending on the intensity of GCaMP6s expression. Data acquisition started after the adjustment of imaging parameters. The animal was kept habituated to the microscope for additional > 5 minutes to obtain background signal, and then the intruder male animal was introduced to the subject's home cage. Calcium activity as well as animal behavior was recorded until 2-10 minutes after the completion of mating. Imaging data were spatially down-sampled by factor of 4 and temporally down-sampled to 10 Hz using the Inscopix Data Processing software (1.8.0). The data was further filtered by a spatial band-pass filter and motion corrected using the same software. Masks were manually drawn to extract data from single cell. The data frame containing GCaMP6s signal intensity traces were exported from the Inscopix Data Processing software and further processed in Python. Signal intensity array was z-scored using the background signal. For peri event activity analysis in **Figure 3** and **Figure 4**, z-scored signal was collected from -5 to + 15 seconds around the behavior onset. Peri event activity from multiple behavior events were concatenated and averaged. Finally, the mean value of pre-behavior background (-5 to 0 seconds from onset) was subtracted. The magnitude of z-scored signal was quantified by averaging 0 to +5 seconds from onset. Cells that had larger than 2 d z-scored signal were classified as "responding" cells. For persistent activity analysis in **Figure 5**, z-scored signal was collected from -5 to + 120 seconds around the onset of mating completion. The mean value of pre-behavior background (-5 to 0 seconds from onset) was subtracted. The decay length was quantified by calculating the time the z-scored signal was smaller than 0. The magnitude of z-scored signal was quantified by averaging 0 to +5 seconds from onset. Spectral clustering was conducted using scikit-learn package and previously used custom script (Namboodiri et al., 2019). Briefly, first dimensionality reduction using principal component analysis was conducted for z-scored signal from -5 to +120 seconds around the onset of mating completion. Next, n = 4 principal components were used to project the data. This was further used as the input into the clustering

algorithm while systematically testing nearest neighbor and number of cluster variables. The best variable that resulted in maximizing the silhouette score was determined (number of clusters = 5, number of nearest neighbors = 55, average silhouette score = 0.405). All clusters contained cells from multiple animal subjects, indicating the variability of the dataset can be explained by heterogenous cell population, rather than subject variability.

TRAP experiments.

TRAP method was conducted as previously described with modifications (DeNardo et al., 2019). TRAP2::Ai14 or TRAP2 mice were OVX during isoflurane anesthesia and AAV injected if necessary. After 2 – 3 weeks from OVX surgery, animals were prepared for the activity labeling assay. Female subjects were subcutaneously (s.c.) injected with 0.1 mL and 0.05 mL Estradiol (E8515, Sigma-Aldrich, 0.1 mg/ml) dissolved in sesame oil (Sigma-Aldrich) at 24 and 48h before assay. On the day for the assay, female subjects were isolated in their home cage and introduced with a male intruder to either experience appetitive behaviors or mating completion. For the appetitive group, the male intruder was removed after 10–20 minutes. To ensure that the female subject did not experience any consummatory behavior from the male, the male intruder was removed whenever an attempt to mount was observed. For the completion group, the male intruder was removed just after the completion of mating. Immediately after the removal of the male animal, the female subject was I.P. injected with 0.125 mL of 50 mg/kg of 4-Hydroxytamoxifen (Sigma-Aldrich, cat#H6278) dissolved in sesame oil. After the injection, the female subject was isolated in their home cage and kept in the behavior room for overnight to avoid background stimulation. On the following day, the mice were returned to the regular housing.

HCR experiments and analysis.

Hybridization chain reaction (HCR) was performed based on the protocol provided by Molecular Instruments with some modifications (**Figure S3** and **Figure S7E–H**). For *Fos* activity analysis (**Figure S3**), the female subject was first singly housed in the home cage for 1 hour. The male intruder was introduced into the home cage and animal behavior was recorded. For the appetitive group, the male intruder was removed after 10–20 minutes until they first attempt mounting to the female subject. For the completion group, the male intruder was removed just after the completion of mating. Twenty-minutes after the removal of the male intruder, the female subject was immediately sacrificed to collect brain tissue. The brain tissue was then snap-frozen using dry ice. Every fifth 20-micron coronal sections containing the MPOA (3 sections from Bregma +0.10 mm to – 0.10 mm) were collected on a slide glass and fixed with 4% PFA in PBS for 30 min and rinsed with PBS, followed by dehydration with a series of 50%, 70%, 100%, 100% of ethanol. After final dehydration the slides were dried. The tissue was treated with Protease4 (ACDBiosystem) for 5–7 minutes. The slides were then rinsed with PBS and were applied with hybridization buffer (Molecular Instruments) for 10 minutes at 37°C for pre-hybridization. RNA probes for *Fos, Vgat, Vglut2, Calcr, Esr1, Gal, Nts, Prlr* (1 mM, Molecular Instruments) were diluted in a ratio of 1:100–1:250 into the hybridization buffer. After pre-hybridization, hybridization buffer (70 µl) containing the probes was applied to each slide on which the parafilm cover was placed. After 12h–18h of incubation at 37°C in the moisture chamber, the sections were washed, with a series of probe wash buffer and SSC-T buffer (5x SSC, 0.1% Tween 20) mixture. After the final wash, the sections were incubated in amplification buffer (Molecular Instruments) for 30 minutes at room temperature for pre-amplification. Amplification hairpin probes (3 mM, Molecular Instruments) were diluted in a ratio of 1:50 into the hybridization and then snap cooled for 1.5 minutes in 95ºC. After pre-amplification, amplification buffer containing hairpin probes (70 µl) was applied to each slide on which the parafilm cover was placed. After 12h–18h of incubation at room temperature in the moisture chamber, the sections were washed in 5xSSC-T buffer for 30 minutes x2. The sections were quenched for autofluorescence using Vector TrueView reagent (Vector, cat# SP-8400). After

washed in 2xSSC, the sections were stained with DAPI in PBS (5 µg/ml, Thermo Fisher Scientific, cat#D1306) for 8 minutes. The slide was then mounted using Vibrance Antifade Mounting Medium (VECTASHIELD, cat#H-1800). Images were obtained using a conventional microscope (Zeiss, Apotome Imager.M2) with a 20x objective. After image acquisition, the coverslip was removed and washed in 2x SSC for 10 minutes, then incubated with DNase1 (0.25 U/µl, Roche, cat#4716728001) for 1.5 h at room temperature. The section was then washed in 2x SSC for 5 minutes x6. The sections then proceeded to the pre-hybridization step for the next round of HCR. A total of 3 rounds of HCR were conducted. Images from multiple rounds were aligned using HiPlex image registration software (ACDBiosystem) or manually aligned using ImageJ package TrackEM2 (Cardona et al., 2012).

For anatomical characterization for TRAP2 animals used in **Figure S7E–H**, subjects were perfused with PBS and 4% PFA-PBS, then brain was harvested and post-fixed with PFA overnight. Every fourth 40-µm coronal sections containing the MPOA were collected on a slide glass. The sections went through 1 round of HCR and were stained for *Vgat* and *Vglut2* following the procedures described above.

The images with each probe signal were aligned to the DAPI channel to identify MPOA subregions and adjacent regions. The image was processed in HALO v3.2 software (Indica Labs) to segment each cell based on the DAPI signal and to quantify RNA transcript signal in each cell. Parameters for detecting puncta and intensity of each gene were manually adjusted for each tissue section of each animal by a volunteer blind to the experimental condition. The cutoff value to determine a gene "expressing cell" was defined as the mean fluorescent intensity of 3 to 5 transcripts depending on the background fluorescent signal. For supervised clustering of the MPN cell gene expression matrix (**Figure S3K–M**) was conducted using Seurat3.1.1 in R. Cells that had no mRNA signal were excluded from the dataset. This expression matrix contained single cells detected across all 10 animals and the spot counts for every gene; we also included signal intensity measurements as metadata. Once loaded, the HCR digital expression matrix was scaled but not normalized. During scaling, we regressed out gene intensity measurements on the basis that signal intensity may indicate staining quality. Next, cells were clustered using the same pipeline. The cells were UMAP plotted using nearest_neighbors = 100, minimum_distance = 0.05 (**Figure S3K**). The cluster ID for each cell was exported and used for statistical analysis using custom Python scripts.

Immunohistochemistry experiments.

To evaluate the accuracy and efficiency of TRAP labeling, we utilized subjects used in pharmacogenetic experiments (**Figure 6, Figure S7**) and labeled neurons that respond to mating completion using immunohistochemistry against immediate early gene c-Fos. The TRAP2 female subjects were labeled with eYFP or hM3Dq-mCherry in the appetitive or mating completion responding neurons in the MPOA (Appetitive-hM3Dq group, Completion-hM3Dq or Completion-eYFP group). Ninety-minutes before perfusion, the female subjects experienced mating completion during a home cage mating assay (described in "**Behavior experiments and analysis**.") to activate the mating completion responding neurons in the MPOA. The subjects were then perfused with PBS and 4% PFA-PBS, and the brain was harvested and post-fixed with PFA overnight. Every fourth 40-µm coronal sections containing the MPOA were collected. were washed three times with PBS-T (1x PBS, 0.3% Triton-X, Sigma-Aldrich, cat# 11332481001) for 10 min x3, and treated with 5% normal donkey serum (NDS, Sigma-Aldrich, cat# 566460) in PBST for 1 hr at room temperature for blocking. Sections were then incubated with rabbit anti-cFos antibody (Abcam, cat#190289-Rb, 1:500), diluted into 5% BSA in PBST for overnight at 4°C. Antibody signals were detected by goat anti-rabbit Alexa 488 or Alexa 594 (Invitrogen, cat#A21206 or cat#A21209, 1:500) for 2h at room temperature. Sections were washed once with

PBST for 10 min, treated with PBS containing DAPI for 20 min, rinsed with PBS, and mounted with cover glass using Vibrance Antifade Mounting Medium (VECTASHIELD, cat#H-1800).

Sections were imaged by FV-3000 confocal microscope (Olympus) with a 20x objective. Images were processed in cellpose to segment DAPI positive cells in the MPOA and their subregions (Stringer et al., 2021). DAPI positive cell masks were used to quantify intensity of c-Fos protein or YFP/mCherry signal. The intensity value was used to determine the negative and positive cell.

Brain-wide analysis of activity-dependent labeling experiments.

TRAP2::Ai14 females were used to label neurons responding to appetitive behavior or mating completion. Two-weeks after activity labeling (described in "**TRAP experiments.**"), the animals were perfused with PBS and 4% PFA-PBS, the brain was harvested and post-fixed with PFA overnight. After post-fixation, the brains were processed for tissue clearing. For tissue clearing, we utilized stabilization under harsh conditions via intramolecular epoxide linkages to prevent degradation method (SHIELD) (Park et al., 2019). The procedures followed the SHIELD tissue clearing protocol (Full Active Pipeline Protocol v5.05, LifeCanvas). Briefly, the brain was incubated in SHIELD OFF solution [2.5 mL DI water, 2.5 mL SHIELD-Buffer Solution, 5 mL SHIELD-Epoxy Solution] at 4oC for 4 days. Then transferred to SHIELD ON buffer and incubated at 37°C for 24 hrs. Following, SHIELD ON buffer incubation, the brain was pre-incubated in Delipidization buffer for overnight at room temperature. The tissue was then placed into SmartClear II Pro (LifeCanvas) to conduct active tissue clearing for 24 hours. To match the refraction index, the tissue was incubated in 50% of EASYINDEX solution (RI = 1.52, LifeCanvas) at 37ºC shaking for 24 hrs and then 100% of EASYINDEX solution at 37ºC shaking for 24 hrs. The tissue was then embedded in EASYINDEX with 2% agar and mounted onto SmartSPIM light sheet microscope (LifeCanvas). The tissue was mounted ventral side facing toward the objective, imaged from the horizontal view using a 3.6x objective with 4-µm zstep. 594 nm channel was collected as the signal channel, 488 or 647 nm channel was collected as the background channel. Background channel was used for the alignment to the brain atlas. The images were first destriped and then stitched using a custom written script (LifeCanvas). The images were pre-processed and down sampled by 2 times (final resolution (x,y,z) = (3.6 µm, 3.6 µm, 4 µm)). Images were registered to a standard brain atlas Unified Anatomical Atlas (Yongsoo Kim Lab) (resolution (x,y,z) = (20 µm, 20 µm, 50 µm)) using ClearMap pipeline on a cloud-based cluster computer (Chon et al., 2019; Madangopal et al., 2022; Renier et al., 2016). tdTomato expressing cells were segmented through the same pipeline using a classifier created using Ilastik (Berg et al., 2019). To train the classifier, 10 chunks of images from the 4 of the subjects were randomly sampled and used as the training dataset (Image size, (x,y,z) = 1.8 mm x 1.8 mm x 100 µm). One chunk image of the same size from each subject was used as the test dataset. The quality of the classifier was visually examined. The total number of tdTomato positive cells per brain region was quantified and normalized by the size of each brain region (density, mm^3). In the standard brain atlas, brain regions were hierarchically sorted from broader regions to finer regions (level 1 to level 8). Level 4 was selected for broader analysis of brain regions (**Figure 2C**). Level 6 was selected for finer analysis of brain regions (**Figure 2I, Figure S2**). To compare the means of density of tdTomato cell in each brain area between the Appetitive group and Completion group, we conducted Student's t-test and further corrected for multiple comparisons with Benjamini/Hochberg correction. False discovery rate (FDR) = 0.05 was used for the broader analysis while a loose discovery rate (FDR = 0.10) was used for finer analysis due to the large number of comparisons.

Quantification, data processing and Statistical Analysis.

Data were presented as mean with error bar of 95% confidence interval unless otherwise mentioned. Data processing and plot generation was done in Python and R. Plots were further

processed in Adobe Illustrator to create Figures. The sample sizes were chosen based on previous studies using similar behavioral experiments. Codes used for analysis and statistics are provided on Github (https://github.com/stuberlab/Ishii-Mating-completion.git). The statistical details of each experiment including the statistical tests used, exact value of n and what n represents, are shown in each figure legend. Each statistical test result is shown in **Table 1**. Significance was shown as *$p < 0.05$, **$p < 0.01$, ***$p < 0.001$ and not significant values were not noted or shown as n.s.

Author Contributions:

Experiments were conceived and designed by K.K.I. and G.D.S. G.D.S. supervised the project, provided resources, and funding. K.H. provided transcriptional analysis data of the MPOA and assisted in gene selection of HCR experiments. J.C. conducted HCR experiments and histological analysis. S.Y., R.E.F. and S.K. conducted behavioral experiments as well as behavioral annotations. C.Z. provided *in vivo* imaging data analysis pipelines. J.N., A.D.M, E.R.S., and S.A.G. assisted and supervised tissue clearing experiments and whole-brain data analysis.

Acknowledgments:

This work was supported by a JSPS oversea fellowship (K.K.I.), Uehara postdoctoral fellowship (K.K.I.), NIH grants R37 DA032750, R01 DA038168, R01 DA054317, P30 DA048736 and Washington Research Foundation Postdoctoral Fellowship (E.R.S.)

References:

Agrati D. 2022. Adolescence and Postpartum: Two Life Periods to Deepen Our Understanding of the Complexity of Female Rat Sexual Behavior. *Sexes* **3**:282–297. doi:10.3390/sexes3020022

Berg S, Kutra D, Kroeger T, Straehle CN, Kausler BX, Haubold C, Schiegg M, Ales J, Beier T, Rudy M, Eren K, Cervantes JI, Xu B, Beuttenmueller F, Wolny A, Zhang C, Koethe U, Hamprecht FA, Kreshuk A. 2019. ilastik: interactive machine learning for (bio)image analysis. *Nature Methods* **16**:1226–1232. doi:10.1038/s41592-019-0582-9

Cardona A, Saalfeld S, Schindelin J, Arganda-Carreras I, Preibisch S, Longair M, Tomancak P, Hartenstein V, Douglas RJ. 2012. TrakEM2 Software for Neural Circuit Reconstruction. *PLoS ONE* **7**:e38011. doi:10.1371/journal.pone.0038011

Chapman T, Bangham J, Vinti G, Seifried B, Lung O, Wolfner MF, Smith HK, Partridge L. 2003. The sex peptide of Drosophila melanogaster: Female post-mating responses analyzed by using RNA interference. *Proceedings of the National Academy of Sciences* **100**:9923–9928. doi:10.1073/pnas.1631635100

Chen PS, Stumm-Zollinger E, Aigaki T, Balmer J, Bienz M, Böhlen P. 1988. A male accessory gland peptide that regulates reproductive behavior of female D. melanogaster. *Cell* **54**:291–298. doi:10.1016/0092-8674(88)90192-4

Choi HMT, Beck VA, Pierce NA. 2014. Next-Generation in Situ Hybridization Chain Reaction: Higher Gain, Lower Cost, Greater Durability. *ACS Nano* **8**:4284–4294. doi:10.1021/nn405717p

Chon U, Vanselow DJ, Cheng KC, Kim Y. 2019. Enhanced and unified anatomical labeling for a common mouse brain atlas. *Nature Communications* **10**. doi:10.1038/s41467-019-13057-w

Dai B, Sun F, Tong X, Ding Y, Kuang A, Osakada T, Li Y, Lin D. 2022. Responses and functions of dopamine in nucleus accumbens core during social behaviors. *Cell Reports* **40**:111246. doi:10.1016/j.celrep.2022.111246

DeNardo LA, Liu CD, Allen WE, Adams EL, Friedmann D, Fu L, Guenthner CJ, Tessier-Lavigne M, Luo L. 2019. Temporal evolution of cortical ensembles promoting remote memory retrieval. *Nat Neurosci* **22**:460–469. doi:10.1038/s41593-018-0318-7

Dimén D, Puska G, Szendi V, Sipos E, Zelena D, Dobolyi Á. 2021. Sex-specific parenting and depression evoked by preoptic inhibitory neurons. *iScience* **24**:103090. doi:10.1016/j.isci.2021.103090

Erskine MS. 1989. Solicitation behavior in the estrous female rat: A review. *Hormones and Behavior* **23**:473–502. doi:10.1016/0018-506X(89)90037-8

Fang Y-Y, Yamaguchi T, Song SC, Tritsch NX, Lin D. 2018. A Hypothalamic Midbrain Pathway Essential for Driving Maternal Behaviors. *Neuron* **98**:192-207.e10. doi:10.1016/j.neuron.2018.02.019

Feng K, Palfreyman MT, Häsemeyer M, Talsma A, Dickson BJ. 2014. Ascending SAG Neurons Control Sexual Receptivity of Drosophila Females. *Neuron* **83**:135–148. doi:10.1016/j.neuron.2014.05.017

Flanigan ME, Kash TL. 2022. Coordination of social behaviors by the bed nucleus of the stria terminalis. *Eur J of Neuroscience* **55**:2404–2420. doi:10.1111/ejn.14991

Franklin KBJ, Paxinos G. 2007. The mouse brain in stereotaxic coordinates. Academic Press.

Friard O, Gamba M. 2016. BORIS: a free, versatile open-source event-logging software for video/audio coding and live observations. *Methods in Ecology and Evolution* **7**:1325–1330. doi:10.1111/2041-210X.12584

Gillott C. 2003. Male Accessory Gland Secretions: Modulators of Female Reproductive Physiology and Behavior. *Annual Review of Entomology* **48**:163–184. doi:10.1146/annurev.ento.48.091801.112657

Hashikawa K, Hashikawa Y, Falkner A, Lin D. 2016. The neural circuits of mating and fighting in male mice. *Current Opinion in Neurobiology* **38**:27–37. doi:10.1016/j.conb.2016.01.006

Hashikawa K, Hashikawa Y, Liu Y, Rossi MA, Basiri ML, Chen JY, Ahmad OR, Mukundan RV, Johnston NL, McHenry JA, Palmiter RD, Rubinow DR, Zweifel LS, Stuber GD. 2021. Pubertal sex hormones control transcriptional trajectories in the medial preoptic area. *bioRxiv* **1**:2021.09.02.458782.

Hull EM, Wood RI, McKenna KE. 2005. Neurobiology of Male Sexual BehaviorKnobil and Neill's Physiology of Reproduction. Elsevier. pp. 1729–1824. doi:10.1016/B978-012515400-0/50038-5

Inoue S, Yang R, Tantry A, Davis C ha, Yang T, Knoedler JR, Wei Y, Adams EL, Thombare S, Golf SR, Neve RL, Tessier-Lavigne M, Ding JB, Shah NM. 2019. Periodic Remodeling in a Neural Circuit Governs Timing of Female Sexual Behavior. *Cell* **179**:1393-1408.e16. doi:10.1016/j.cell.2019.10.025

Ishii KK, Osakada T, Mori H, Miyasaka N, Yoshihara Y, Miyamichi K, Touhara K. 2017. A Labeled-Line Neural Circuit for Pheromone-Mediated Sexual Behaviors in Mice. *Neuron* **95**:123-137.e8. doi:10.1016/j.neuron.2017.05.038

Ishii KK, Touhara K. 2018. Neural circuits regulating sexual behaviors via the olfactory system in mice. *Neuroscience Research*. doi:10.1016/j.neures.2018.10.009

Karigo T, Kennedy A, Yang B, Liu M, Tai D, Wahle IA, Anderson DJ. 2021. Distinct hypothalamic control of same- and opposite-sex mounting behaviour in mice. *Nature* **589**:258–263. doi:10.1038/s41586-020-2995-0

Kato A, Sakuma Y. 2000. Neuronal activity in female rat preoptic area associated with sexually motivated behavior, Brain Research.

Kohl J, Babayan BM, Rubinstein ND, Autry AE, Marin-Rodriguez B, Kapoor V, Miyamishi K, Zweifel LS, Luo L, Uchida N, Dulac C. 2018. Functional circuit architecture underlying parental behaviour. *Nature* **556**:326–331. doi:10.1038/s41586-018-0027-0

Lenschow C, Lima SQ. 2020. In the mood for sex: neural circuits for reproduction. *Current Opinion in Neurobiology* **60**:155–168. doi:10.1016/j.conb.2019.12.001

Liu H, Kubli E. 2003. Sex-peptide is the molecular basis of the sperm effect in Drosophila melanogaster. *Proceedings of the National Academy of Sciences* **100**:9929–9933. doi:10.1073/pnas.1631700100

Liu M, Kim DW, Zeng H, Anderson DJ. 2022. Make war not love: The neural substrate underlying a state-dependent switch in female social behavior. *Neuron* **110**:841-856.e6. doi:10.1016/j.neuron.2021.12.002

Lo L, Yao S, Kim D-W, Cetin A, Harris J, Zeng H, Anderson DJ, Weissbourd B. 2019. Connectional architecture of a mouse hypothalamic circuit node controlling social behavior. *Proceedings of the National Academy of Sciences* **116**:7503–7512. doi:10.1073/pnas.1817503116

Madangopal R, Szelenyi ER, Nguyen J, Brenner MB, Drake OR, Pham DQ, Shekara A, Jin M, Choong JJ, Heins C, Komer LE, Weber SJ, Hope BT, Shaham Y, Golden SA. 2022. Incubation of palatable food craving is associated with brain-wide neuronal activation in mice. *Proc Natl Acad Sci USA* **119**:e2209382119. doi:10.1073/pnas.2209382119

Marsh N, Marsh AA, Lee MR, Hurlemann R. 2021. Oxytocin and the Neurobiology of Prosocial Behavior. *Neuroscientist* **27**:604–619. doi:10.1177/1073858420960111

McGill TE, Coughlin RC. 1970. Ejaculatory reflex and luteal activity induction in Mus musculus. *Journal of reproduction and fertility* **21**:215–220. doi:10.1530/jrf.0.0210215

McHenry JA, Otis JM, Rossi MA, Robinson JE, Kosyk O, Miller NW, McElligott ZA, Budygin EA, Rubinow DR, Stuber GD. 2017. Hormonal gain control of a medial preoptic area social reward circuit. *Nature neuroscience* **20**:449–458. doi:10.1038/nn.4487

Mei L, Yan R, Yin L, Sullivan RM, Lin D. 2023. Antagonistic circuits mediating infanticide and maternal care in female mice. *Nature*. doi:10.1038/s41586-023-06147-9

Micevych PE, Meisel RL. 2017. Integrating Neural Circuits Controlling Female Sexual Behavior. *Frontiers in Systems Neuroscience* **11**:42. doi:10.3389/fnsys.2017.00042

Moffitt JR, Bambah-Mukku D, Eichhorn SW, Vaughn E, Shekhar K, Perez JD, Rubinstein ND, Hao J, Regev A, Dulac C, Zhuang X. 2018. Molecular, spatial, and functional single-cell profiling of the hypothalamic preoptic region. *Science* **362**. doi:10.1126/science.aau5324

Namboodiri VMK, Otis JM, van Heeswijk K, Voets ES, Alghorazi RA, Rodriguez-Romaguera J, Mihalas S, Stuber GD. 2019. Single-cell activity tracking reveals that orbitofrontal neurons acquire and maintain a long-term memory to guide behavioral adaptation. *Nature Neuroscience* **22**:1110–1121. doi:10.1038/s41593-019-0408-1

Nath T, Mathis A, Chen AC, Patel A, Bethge M, Mathis MW. 2019. Using DeepLabCut for 3D markerless pose estimation across species and behaviors. *Nature Protocols* **14**:2152–2176. doi:10.1038/s41596-019-0176-0

Nilson SR, Goodwin NL, Choong JJ, Hwang S, Wright HR, Norville ZC, Tong X, Lin D, Bentzley BS, Eshel N, Mclaughlin RJ, Golden SA. 2020. Simple Behavioral Analysis (SimBA) – an open source toolkit for computer classification of complex social behaviors in experimental animals. doi:10.1101/2020.04.19.049452

Nyuyki KD, Waldherr M, Baeuml S, Neumann ID. 2011. Yes, I Am Ready Now: Differential Effects of Paced versus Unpaced Mating on Anxiety and Central Oxytocin Release in Female Rats. *PLoS ONE* **6**:e23599. doi:10.1371/journal.pone.0023599

Osakada T, Ishii KK, Mori H, Eguchi R, Ferrero DM, Yoshihara Y, Liberles SD, Miyamichi K, Touhara K. 2018. Sexual rejection via a vomeronasal receptor-triggered limbic circuit. *Nature communications* **9**:4463. doi:10.1038/s41467-018-07003-5

Parada M, Chamas L, Censi S, Coria-Avila G, Pfaus JG. 2010. Clitoral stimulation induces conditioned place preference and Fos activation in the rat. *Hormones and Behavior* **57**:112–118. doi:10.1016/j.yhbeh.2009.05.008

Parada M, Sparks LM, Censi S, Pfaus JG. 2014. Clitoral anesthesia disrupts paced copulation in the female rat. *Physiology & Behavior* **123**:180–186. doi:10.1016/j.physbeh.2013.10.018

Park Y-G, Sohn CH, Chen R, McCue M, Yun DH, Drummond GT, Ku T, Evans NB, Oak HC, Trieu W, Choi H, Jin X, Lilascharoen V, Wang J, Truttmann MC, Qi HW, Ploegh HL, Golub TR, Chen S-C, Frosch MP, Kulik HJ, Lim BK, Chung K. 2019. Protection of tissue physicochemical properties using polyfunctional crosslinkers. *Nature Biotechnology* **37**:73–83. doi:10.1038/nbt.4281

Peirce JT, Nuttall DL. 1961. Self-paced sexual behavior in the female rat. *Journal of Comparative and Physiological Psychology* **54**:310–313. doi:10.1037/h0040740

Pfaff DW, Sakuma Y. 1979a. Deficit in the lordosis reflex of female rats caused by lesions in the ventromedial nucleus of the hypothalamus. *The Journal of physiology* **288**:203–210. doi:10.1113/jphysiol.1979.sp012690

Pfaff DW, Sakuma Y. 1979b. Facilitation of the lordosis reflex of female rats from the ventromedial nucleus of the hypothalamus. *The Journal of physiology* **288**:189–202. doi:10.1113/jphysiol.1979.sp012690

Pfaus JG, Kleopoulos SP, Mobbs CV, Gibbs RB, Pfaff DW. 1993. Sexual stimulation activates c-fos within estrogen-concentrating regions of the female rat forebrain. *Brain Research* **624**:253–267. doi:10.1016/0006-8993(93)90085-2

Pfaus JG, Marcangione C, Smith WJ, Manitt C, Abillamaa H. 1996. Differential induction of Fos in the female rat brain following different amounts of vaginocervical stimulation: modulation by steroid hormones. *Brain Research* **741**:314–330. doi:10.1016/S0006-8993(96)00985-7

Powers B, Valenstein ES. 1972. Sexual receptivity: facilitation by medial preoptic lesions in female rats. *Science (New York, NY)* **175**:1003–5.

Raam T, Hong W. 2021. Organization of neural circuits underlying social behavior: A consideration of the medial amygdala. *Current Opinion in Neurobiology* **68**:124–136. doi:10.1016/j.conb.2021.02.008

Renier N, Adams EL, Kirst C, Wu Z, Azevedo R, Kohl J, Autry AE, Kadiri L, Umadevi Venkataraju K, Zhou Y, Wang VX, Tang CY, Olsen O, Dulac C, Osten P, Tessier-Lavigne M. 2016. Mapping of Brain Activity by Automated Volume Analysis of Immediate Early Genes. *Cell* **165**:1789–1802. doi:10.1016/j.cell.2016.05.007

Rezával C, Pavlou HJ, Dornan AJ, Chan Y-B, Kravitz EA, Goodwin SF. 2012. Neural Circuitry Underlying Drosophila Female Postmating Behavioral Responses. *Current Biology* **22**:1155–1165. doi:10.1016/j.cub.2012.04.062

Stringer C, Wang T, Michaelos M, Pachitariu M. 2021. Cellpose: a generalist algorithm for cellular segmentation. *Nature Methods* **18**:100–106. doi:10.1038/s41592-020-01018-x

Troconis EL, Seo C, Guru A, Warden MR. 2023. Male ejaculation phasically activates dorsal raphe serotonin neurons in mating female mice. doi:10.1101/2023.05.14.540716

Tsuneoka Y, Funato H. 2021. Cellular Composition of the Preoptic Area Regulating Sleep, Parental, and Sexual Behavior. *Frontiers in Neuroscience* **15**. doi:10.3389/fnins.2021.649159

Uphouse L. 2014. Pharmacology of serotonin and female sexual behavior. *Pharmacology Biochemistry and Behavior* **121**:31–42. doi:10.1016/j.pbb.2013.11.008

Wei Y, Wang S, Jiao Z, Zhang W, Lin J, Li X-Y, Li S, Zhang X, Xu X. 2018. Medial preoptic area in mice is capable of mediating sexually dimorphic behaviors regardless of gender. *Nature Communications* **9**:279. doi:10.1038/s41467-017-02648-0

Wu Z, Autry AE, Bergan JF, Watabe-Uchida M, Dulac CG. 2014. Galanin neurons in the medial preoptic area govern parental behaviour. *Nature* **509**:325–30. doi:10.1038/nature13307

Yang CF, Chiang MC, Gray DC, Prabhakaran M, Alvarado M, Juntti SA, Unger EK, Wells JA, Shah NM. 2013. Sexually dimorphic neurons in the ventromedial hypothalamus govern mating in both sexes and aggression in males. *Cell* **153**:896–909. doi:10.1016/j.cell.2013.04.017

Yapici N, Kim YJ, Ribeiro C, Dickson BJ. 2008. A receptor that mediates the post-mating switch in Drosophila reproductive behaviour. *Nature* **451**:33–37. doi:10.1038/nature06483

Yin L, Hashikawa K, Hashikawa Y, Osakada T, Lischinsky JE, Diaz V, Lin D. 2022. VMHvlCckar cells dynamically control female sexual behaviors over the reproductive cycle. *Neuron* **110**:3000-3017.e8. doi:10.1016/j.neuron.2022.06.026

Yoshihara C, Tokita K, Maruyama T, Kaneko M, Tsuneoka Y, Fukumitsu K, Miyazawa E, Shinozuka K, Huang AJ, Nishimori K, McHugh TJ, Tanaka M, Itohara S, Touhara K, Miyamichi K, Kuroda KO. 2021. Calcitonin receptor signaling in the medial preoptic area enables risk-taking maternal care. *Cell Reports* **35**:109204. doi:10.1016/j.celrep.2021.109204

Zhang G-W, Shen L, Tao C, Jung A-H, Peng B, Li Z, Zhang LI, Tao HW. 2021. Medial preoptic area antagonistically mediates stress-induced anxiety and parental behavior. *Nat Neurosci* **24**:516–528. doi:10.1038/s41593-020-00784-3

Zhang SX, Lutas A, Yang S, Diaz A, Fluhr H, Nagel G, Gao S, Andermann ML. 2021. Hypothalamic dopamine neurons motivate mating through persistent cAMP signalling. *Nature* **597**:245–249. doi:10.1038/s41586-021-03845-0

Zhou X, Li A, Mi X, Li Yixuan, Ding Z, An M, Chen Y, Li W, Tao X, Chen X, Li Ying. 2023. Hyperexcited limbic neurons represent sexual satiety and reduce mating motivation. *Science (New York, NY)* **379**:820–825. doi:10.1126/science.abl4038

Figures:

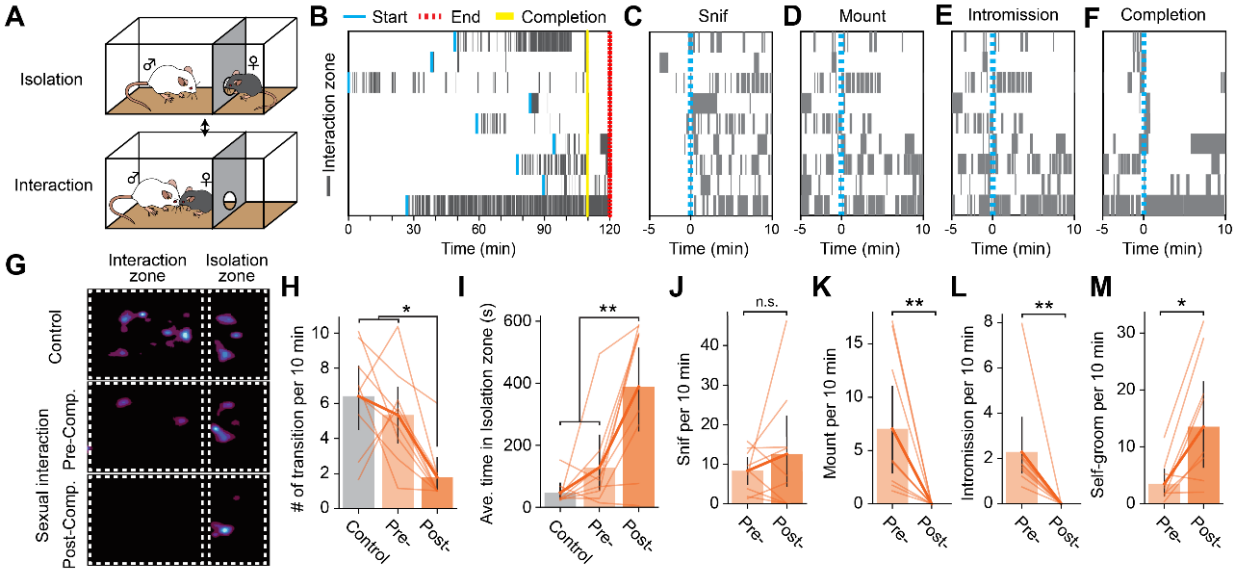

Figure 1: Female mice show decreased sexual motivation after mating completion.

(**A**) Schematic of female self-paced mating assay. The behavior apparatus was divided by a wall with a hole small enough for only the female subject to go through. The female subject was allowed to freely choose between "interaction" with the male intruder in the larger room or "isolation" in the smaller room.

(**B**) Raster plots of time spent in the interaction zone (gray). The onset of mating completion, start and the endpoint of the experiment is shown in yellow, blue and red respectively.

(**C – F**) Raster plots of time spent in the interaction zone (gray) around the onset of the first female to male sniffing, male mounting, intromission and mating completion.

(**G**) Representative heatmap showing the time spent in the behavior apparatus during a control trial or a sexual interaction trial. The sexual interaction trial was further divided into pre- and post-mating completion.

(**H–I**) Number of transitions between the room per 10 minutes (**H**) and the average time spent in the isolation zone (I) during the control trial, and pre- and post- mating completion.

(**J–M**) Number of female to male sniffing (**J**), male mounting (**K**), intromission (**L**) and female self-grooming (**M**) per 10 minutes during pre- and post- mating completion.

All data are shown as mean ± 95% confidence interval and were analyzed by two-way RM ANOVA with Tukey HSD post-hoc test (FWER = 0.05) (**H** and **I**) or Wilcoxon signed-rank test (**J**, **K**, **L** and **M**). n = 9 (**D–K**). $^{*}p < 0.05$, $^{**}p < 0.01$, $^{***}p < 0.001$; ns, not significant.

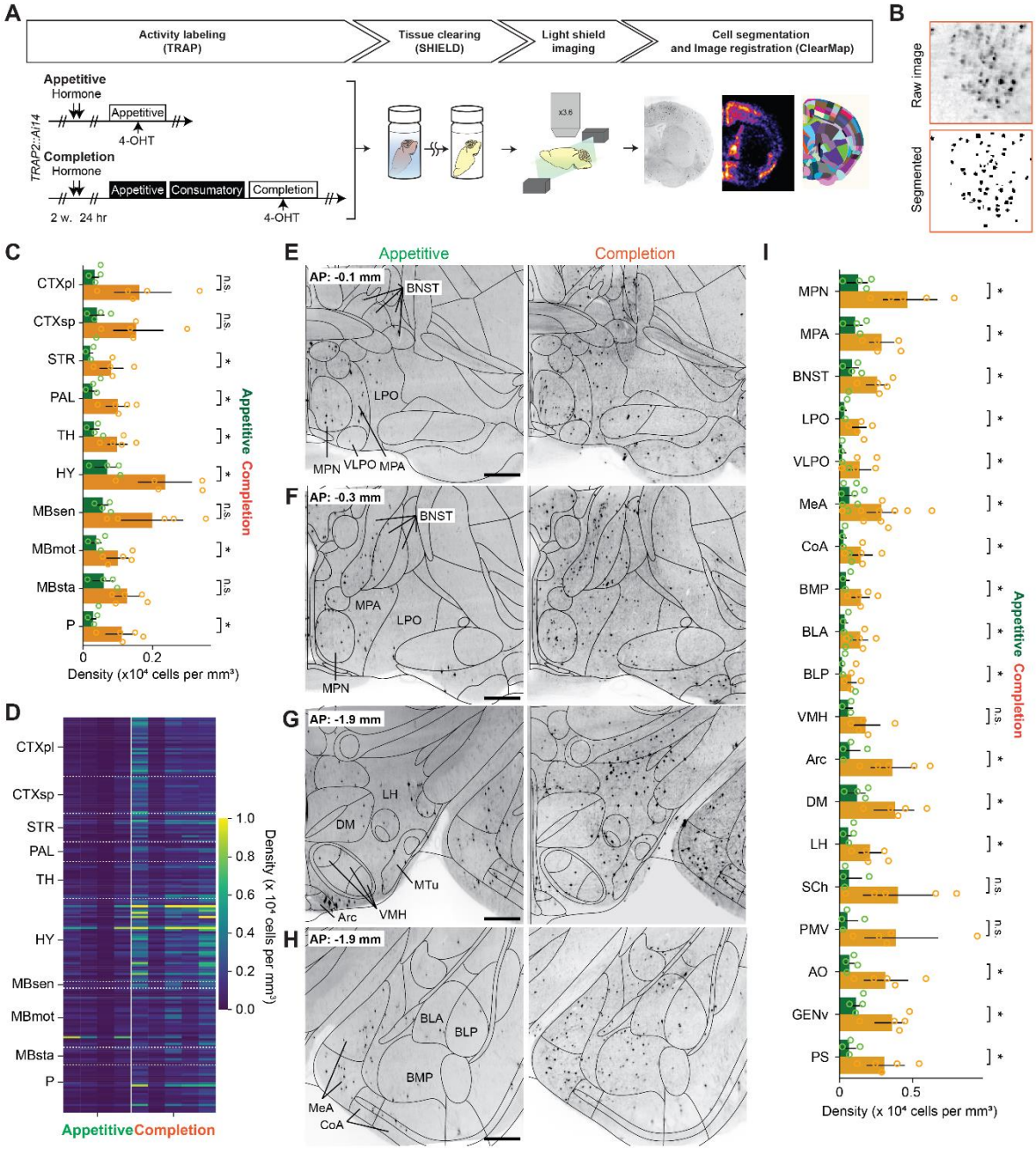

Figure 2: Brain wide analysis of cells responding to mating completion in the female brain. (**A**) Overview of the experiment pipeline. After the activity labeling using TRAP, brain tissue was collected and cleared using SHIELD. The cleared tissue was imaged using a light-sheet microscope. The dataset was registered to a reference brain atlas and the number of tdTomato+ cells were quantified using ClearMap and ilastik.
(**B**) Representative image showing cell segmentation.
(**C**) Density of tdTomato+ cells per mm^3 in larger brain regions. CTXpl: Cortical plate, CTXsp: Cortical subplate, STR: Striatum, PAL: Pallidum, VERM: Vermal regions, HEM: Hemispheric

regions, TH: Thalamus, HY: Hypothalamus, MBsen: Midbrain, sensory related, MBmot: Midbrain, motor related, MBsta: Midbrain, behavioral state related, P: Pons.

(**D**) Heatmap showing density of tdTomato+ cells per mm^3 in subregions. Each column indicates data from one subject. Each row indicates data from one subregion. MPN: Medial preoptic nucleus, MPA: Medial preoptic area, BNST: Bed nuclei of the stria terminalis, LPO: Lateral preoptic area, VLPO: Ventrolateral preoptic nucleus, MeA: Medial amygdaloid nucleus, CoA: cortical amygdaloid nucleus, BMP: Basomedial amygdaloid nucleus, posterior part, BLA: Basolateral amygdaloid nucleus, anterior part, BLP: Basolateral amygdaloid nucleus, posterior part, VMH: Ventromedial hypothalamic nucleus, Arc: Arcuate hypothalamic nucleus, DM: Dorsomedial hypothalamic nucleus, LH: Lateral hypothalamic area, SCh: Suprachiasmatic nucleus, PMV: Premamillary nucleus, ventral part, AO: Anterior olfactory area, GENv: Geniculate group, ventral thalamus, PS: Parastrial nucleus.

(**E-H**) Representative coronal hemisphere image showing expression of tdTomato. Images from Appetitive group are shown in left column, images from Completion group are shown in right. Scale bar 500 μm.

(**I**) Density of tdTomato+ cells per mm^3 in a subset of subregions. The full list of brain regions is shown in **Figure S2.**

All data are shown as mean ± 95% confidence interval and were analyzed by Student's t-test with Benjamini/Hochberg correction (**C**: FDR = 0.05, **I**: FDR = 0.10). Detailed statistical values are shown in **Table 2** and **Table 3.** Appetitive (green), n = 4. Completion (orange), n = 5. $^*p < 0.05$, ns, not significant.

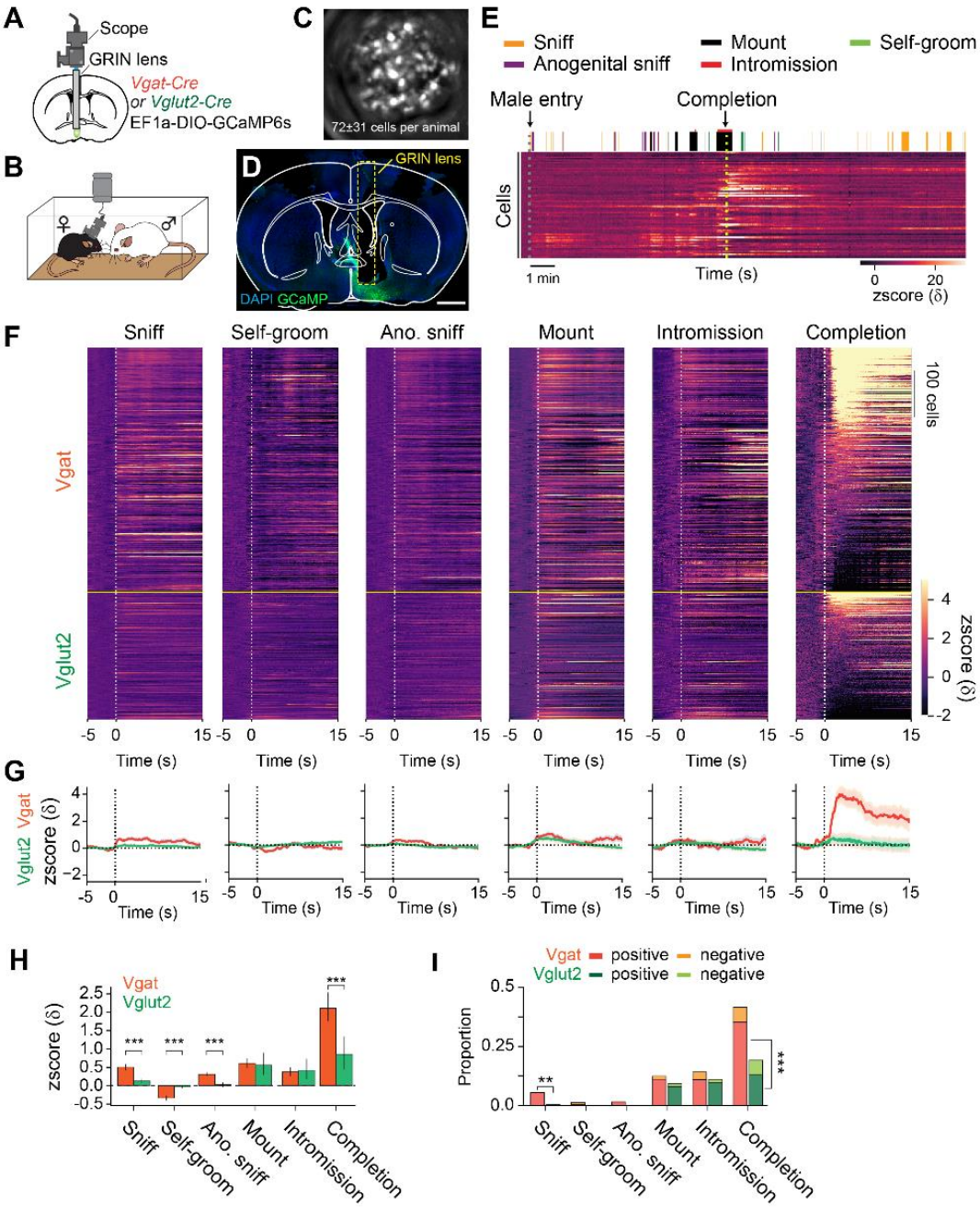

Figure 3 Mating completion signal is strongly represented in the MPOA.
(**A**) Schematic of *in vivo* calcium imaging from MPOA Vgat and Vglut2 neurons. AAVDj EF1a-DIO-GCaMP6s was injected into the MPOA of Vgat-Cre or Vglut2-Cre female mice. A GRIN lens was placed above the MPOA following virus injection.
(**B**) Calcium activity was imaged from a female subject during a free moving mating assay with a sexually experienced male intruder.
(**C**) Representative maximum projected image of the field of view during calcium imaging. Vgat: 87 ± 28 cells, n = 6. Vglut2: 68 ± 42 cells, n = 4.
(**D**) Representative coronal section showing GCaMP6s expression and GRIN lens placement.
(**E**) Representative raster plot showing behavior events during the mating assay and a heatmap showing calcium activity from cells imaged during the assay. Behaviors quantified: female to male

sniffing (Sniff), female self-grooming (Self-groom), male to female anogenital sniffing (Ano. sniff), male mounting (Mount), male intromission (Intromission) and mating completion (Completion).

(**F**) Heatmap showing peri-event calcium activity around behavior onset. Cells are ordered by the average response after mating completion.

(**G**) Line plot showing average calcium activity around behavior onset. Vgat neurons, blue. Vglut cells, orange.

(**H**) Average calcium response magnitude following behavior onset per cell.

(**I**) Proportion of cells which responded positively or negatively to behavior onset (>2δ).

All data are shown as mean ± 95% confidence interval and were analyzed by Student's t-test with Bonferroni correction (**H**) and chisquare test with Bonferroni correction (**I**). $^{*}p < 0.05$, $^{**}p < 0.01$, $^{***}p < 0.001$; ns, not significant.

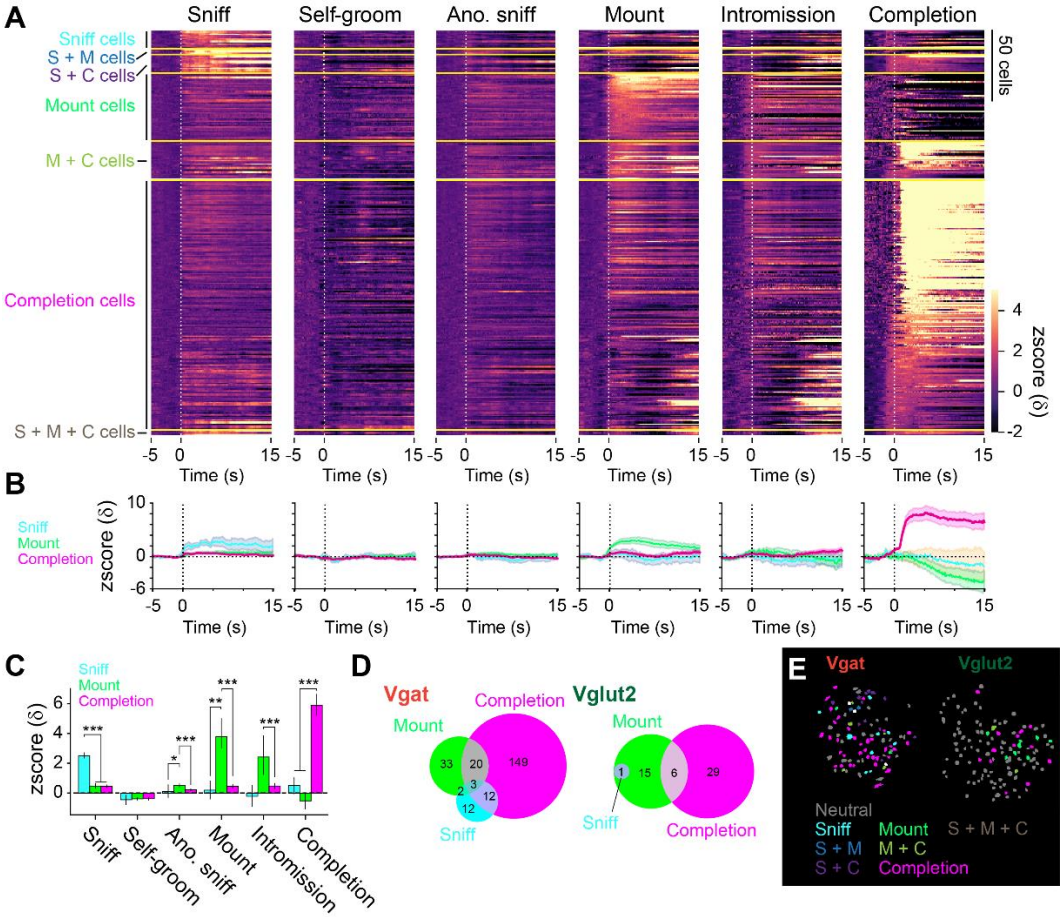

Figure 4: Heterogenous response properties to sexual behaviors in the MPOA.
(**A**) Heatmap showing peri-event calcium activity around behavior onset of cells that were categorized based on response magnitude. S: Sniff, M: Mount, C: Completion.
(**B**) Line plot showing average calcium activity around behavior onset. Sniff cells, blue. Mount cells, green. Completion cells, magenta.
(**C**) Venn diagram showing the number of cells with positive and negative response in each cell type. (>2δ).
(**D**) Average calcium response magnitude following behavior onset per cell in each cell types.
(**E**) Representative field of view showing spatial location of cells with different response properties to sexual behavior in Vgat (left) and Vglut2 (right) cells.
All data are shown as mean ± 95% confidence interval and were analyzed by Student's t-test with Bonferroni correction (**D**). $^{*}p < 0.05$, $^{**}p < 0.01$, $^{***}p < 0.001$; ns, not significant.

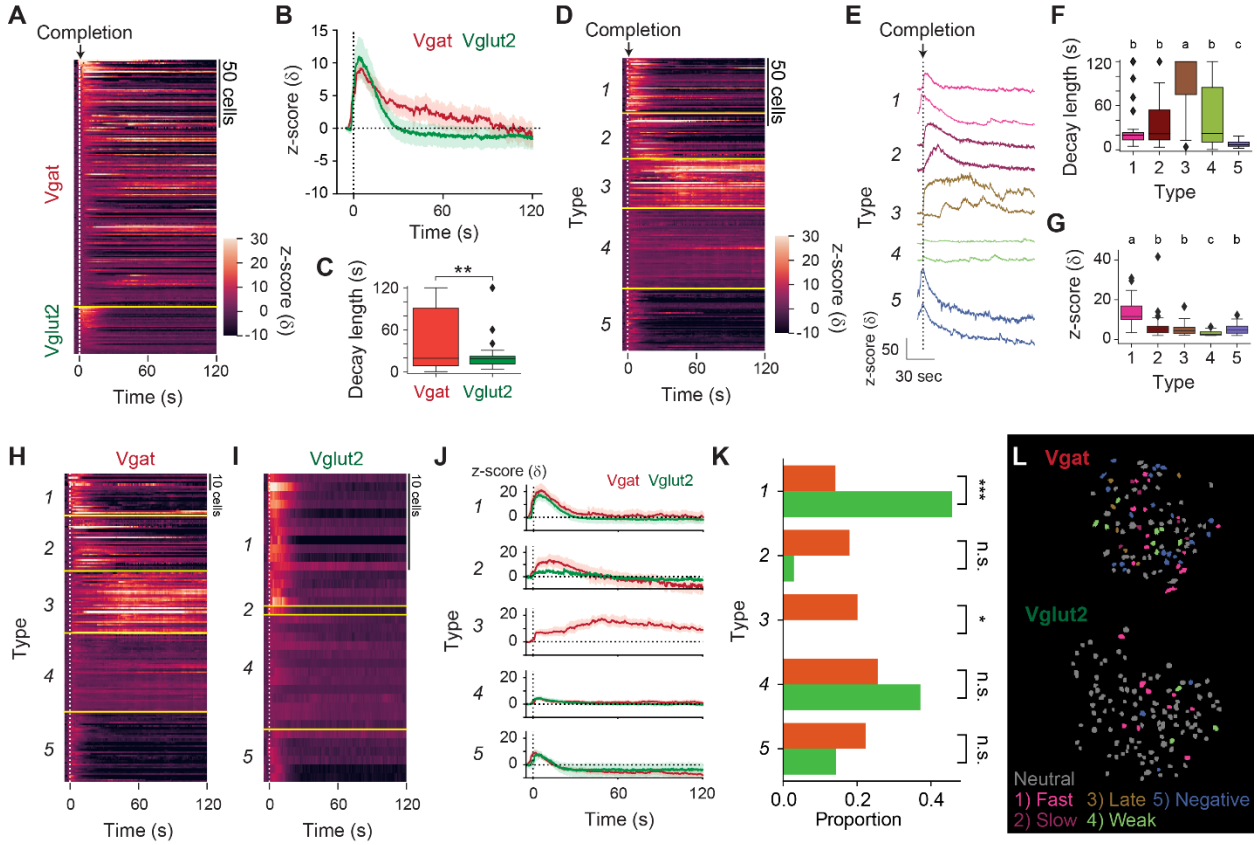

Figure 5 MPOA inhibitory neurons display prolonged activity late after the onset of mating completion in female mice.

(**A**) Heatmap showing peri-event calcium activity around mating completion onset for mating completion-responding cells in a longer time scale.

(**B**) Line plot showing average calcium activity of Vgat and Vglut2 population around behavior onset.

(**C**) The decay length for mating completion-responding cells from Vgat and Vglut2 population.

(**D–G**) Cluster based analysis of the activity pattern of the mating completion-cells.

(**D**) Heatmap showing peri-event calcium activity around mating completion onset sorted by cluster.

(**E**) Representative calcium activity traces of cells from each cluster.

(**F**) The decay length for mating completion-responding cells from each cluster.

(**G**) Average z-scored response for mating completion-responding cells from each cluster.

(**H–K**) Cluster based analysis of the activity pattern of the mating completion-cells in Vgat and Vglut2 population.

(**H–I**) Heatmap showing peri-event calcium activity of Vgat (H) and Vglut2 (I) cells around male ejaculation onset sorted by cluster.

(**J**) Line plot showing average calcium activity of Vgat and Vglut2 cells in each cluster around behavior onset.

(**K**) Proportion of Vgat and Vglut2 cells in each cluster over Vgat and Vglut2 cells in all clusters. Statistical results are shown next to the cluster name. The proportion of type 3 cells in Vgat

population was significantly larger than in Vglut2 ($p<0.05$). The proportion of type 1 cells in Vglut2 population was significantly larger than in Vgat ($p<0.001$).

(**L**) Representative field of view showing spatial location of cells with different response properties after mating completion in Vgat (left) and Vglut2 (right) cells

All data are shown as mean ± 95% confidence interval and were analyzed by Student's t-test (C), two-way ANOVA with post-hoc Tukey HSD test (F and G), and chisquare test with Bonferroni correction (K). (C and K) $^{*}p < 0.05$, $^{**}p < 0.01$, $^{***}p < 0.001$; ns, not significant. (F and G) a vs. b: $p < 0.001$. b vs. c: $p < 0.05$. a vs. c: $p < 0.001$.

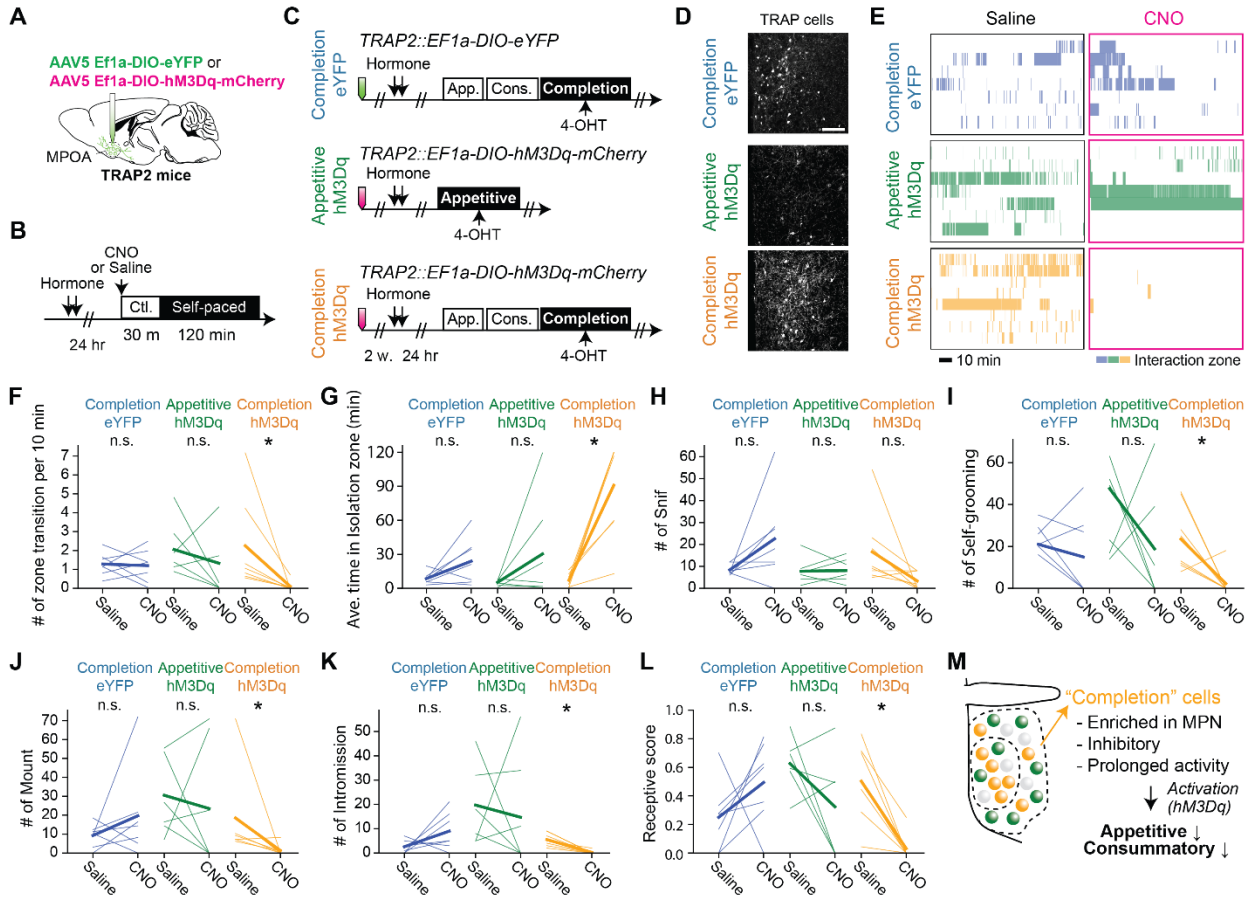

Figure 6: Activation of a subpopulation of MPOA labeled following mating is sufficient to suppress female sexual behavior.

(**A**) Schematic of selective labeling of MPOA neurons using TRAP2. AAV5 EF1a-DIO-hM3Dq-mCherry or AAV5 EF1a-DIO-eYFP as control was injected into the MPOA of the female TRAP2 subjects. After incubation of the virus, the female subjects went through procedures to TRAP cells in MPOA (further described in **C**).

(**B**) Schematic of pharmaco-genetic activation of MPOA neurons during a female self-paced mating assay. Female subjects were primed with hormone before the experiment day. On the experiment day, subjects were injected i.p. with CNO to activate TRAP cells, or saline as control.

30 minutes after the injection, the male intruder was placed into the apparatus and the animal behavior was recorded for 2 hrs.

(**C**) After incubation of the virus, the female subjects were administered with hormones, then received an ejaculation from the male intruder or only interacted without mating. Immediately after, the subjects were administrated with 4-hydroxytamoxifen (4-OHT).

(**D**) Representative image showing TRAP cells MPN from Completion-eYFP, Appetitive-hM3Dq and Completion-hM3Dq group. Further histological analysis is shown in **Figure S7**. Scale bar, 100 μm.

(**E**) Raster plots of time spent in the interaction zone the female self-paced mating assay (Completion-eYFP: blue. Appetitive-hM3Dq: green, Completion-hM3Dq: orange).

(**F–M**) Number of zone transitions per 10 minutes (**F**), average time in isolation zone (**G**), number of female-to-male sniff (**H**), female self-grooming (**I**), male mount (**J**), male intromission (**K**), the receptive score (number of mount episodes with intromissions/number of all mount episodes) (**L**).

(**M**) Schematic illustration summarizing how MPOA neurons suppress female sexual motivation after the completion of mating.

All data are shown by thin lines for individual subjects and thick lines for mean. The data were analyzed by Wilcoxon rank sum test with Bonferroni correction (**F–L**). Completion-eYFP: n = 6, Appetitive-hM3Dq: n = 7, Completion-hM3Dq: n = 8. $^{*}p < 0.05$, $^{**}p < 0.01$, $^{***}p < 0.001$; ns, not significant.

Supplementary Figures:

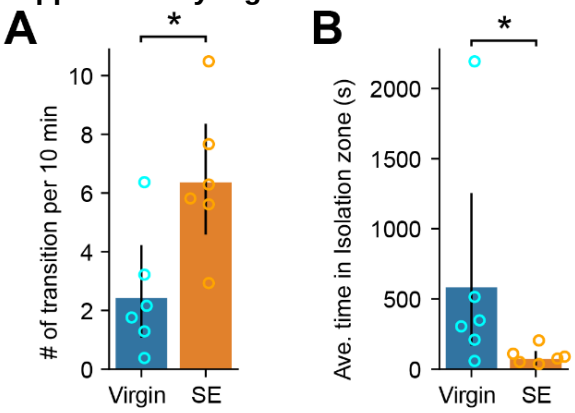

Figure S1: Sexual experience increase sexual motivation in female mice, related to Figure 1.

(**A**) The number of entries in the isolation zone per 10 minutes (**B**) and the average time spent in the isolation zone between virgin animals and sexually experienced animals. All data are shown as mean ± 95% confidence interval and were analyzed by Mann-Whitney U test (**A** and **B**). Virgin: n = 6, SE: n = 6. *p < 0.05, **p < 0.01, ***p < 0.001; ns, not significant.

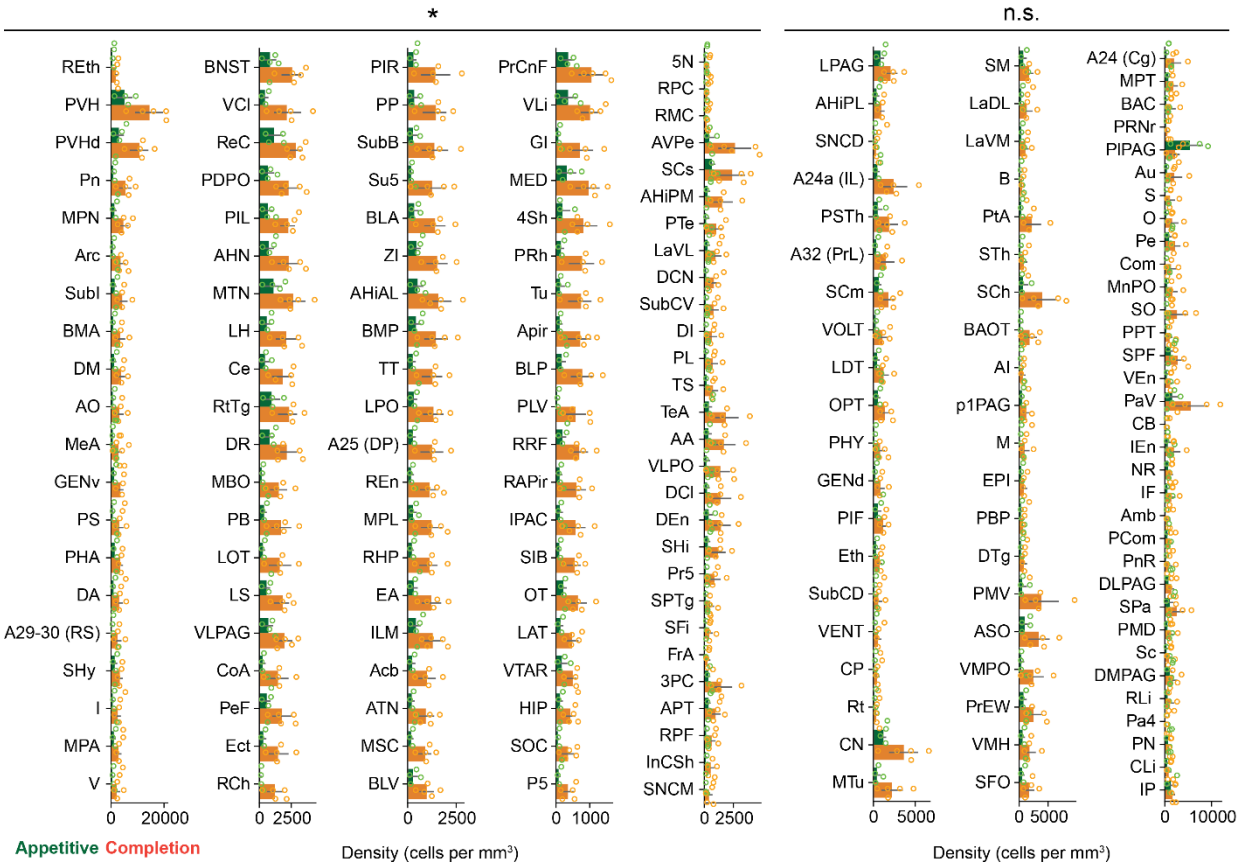

Figure S2: Brain-wide analysis of Completion-responding cells in the female brain related to Figure 2 and Table 3.

Density of tdTomato+ cells in each brain region from Completion group and Appetitive group. Statistical significances are shown above each column. The regions are sorted from the top left to bottom right by the qvalue and then the difference in the density between Completion group and Appetitive group. Detail of statistical values and full name of acronyms are shown in **Table 3**. Appetitive, n = 4. Completion, n = 5. Student's t-test with Benjamini/Hochberg correction (FDR = 0.10), *$p < 0.05$; ns, not significant.

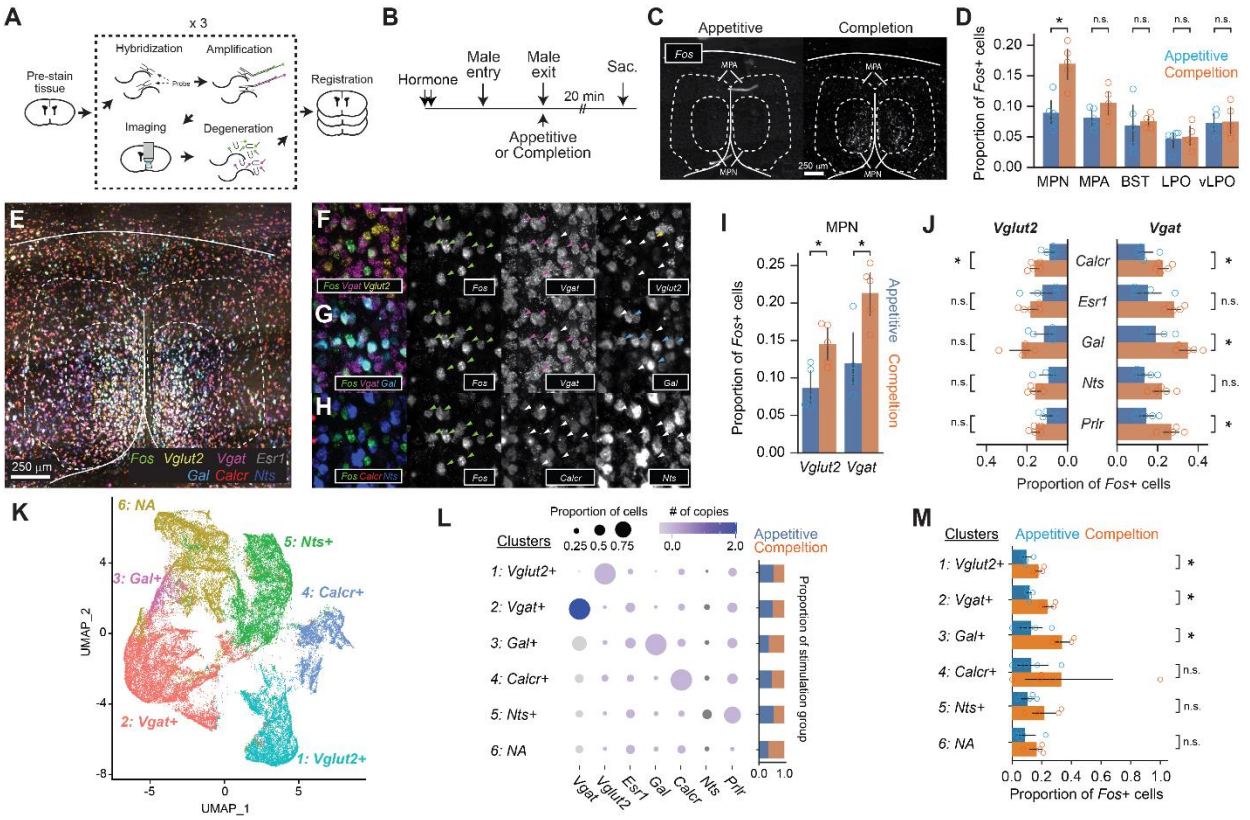

Figure S3: Mating completion labeled cells are composed of a subset of excitatory and inhibitory cells in the MPOA.

(**A**) Brain sections went through multiplexed *in situ* RNA hybridization chain reaction (HCR) to identify cell type markers of MPOA and an immediate early gene *Fos. Vgat, Vglut2, Esr1, Gal, Calcr, Nts, Prlr* were used as cell type markers.

(**B**) Schematic of tissue sampling for *Fos* expression analysis in the MPOA. Wild type female subjects were administered with hormones before the experiment day. On the experiment day, male intruders entered the female home cage. Male intruders were removed immediately after the completion of mating (Completion group) or during the appetitive phase (Appetitive group). Brain tissue was harvested 20 minutes after the male exit.

(**C**) Representative coronal section showing *Fos* mRNA expression in the MPOA of Appetitive and Completion group.

(**D**) Proportion of *Fos*+ cells in each brain subregion. MPN: medial preoptic nucleus, MPA: medial preoptic area, BNST: bed nucleus of stria terminalis, LPO: lateral preoptic area, vLPO: ventral lateral preoptic area.

(**E**) Representative coronal section showing expression of 7 genes: *Fos, Vgat, Vglut2, Esr1, Gal, Calcr, Nts*.

(**F–H**) Expanded image of area highlighted in yellow in (E). (F) Expression of *Fos, Vgat* and *Slc17a6.* (**G**) Expression of *Fos, Vgat* and *Gal.* (H) Expression of *Fos, Calcr* and *Nts.* Colored arrow indicates cells expressing given gene. Scale bar, 50 μm.

(**I**) Proportion of *Vgat*+ or *Vglut2*+ and *Fos*+ cells in the MPN of Appetitive and Completion group.

(**J**) Proportion of *Vgat*+ *Fos*+ or *Vglut2*+ *Fos*+ and cell type marker expressing cells in the MPN of Appetitive and Completion group.

(**K**) UMAP plot of MPN cells.

(**L**) Disc plot showing proportion of gene expressing cell and the number of copies per cell for each gene and cluster. The proportion of cells from each group are shown on the right.
(**M**) Proportion of *Fos*+ cells from Appetitive and Completion group in each cluster.
All data are shown as mean ± 95% confidence interval and were analyzed by Student's t-test with Bonferroni correction (**D, E, K** and **N**). Appetitive group, n = 5. Completion group, n = 5. $^{*}p < 0.05$, $^{**}p < 0.01$, $^{***}p < 0.001$; ns, not significant.

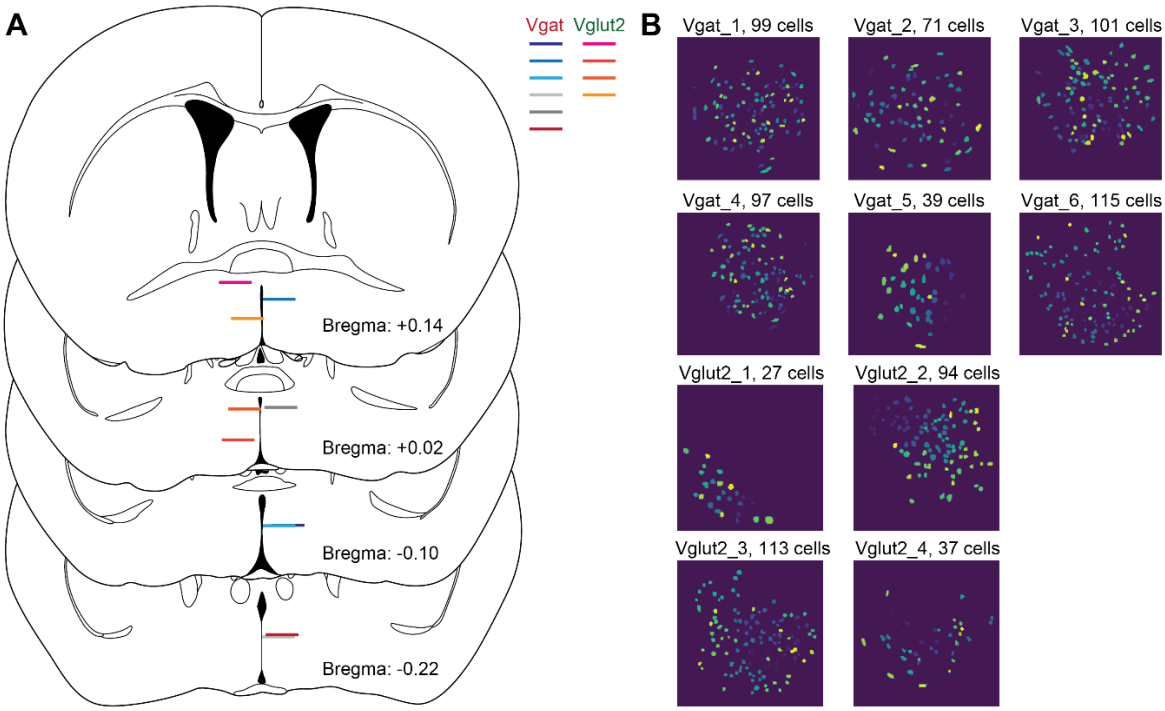

Figure S4: Lens placement and field of view of *in vivo* imaging experiment related to Figure 3, Figure 4, Figure 5.

(**A**) Schematic illustration showing position of GRIN lens placement from each animal. Positions shown on the left hemisphere are from Vglut2 animals, the ones on the right hemisphere are from Vgat animals.

(**B**) Field of view and region of interest (ROI) for each animal. The subject ID and the number of ROI in each FOV are shown above.

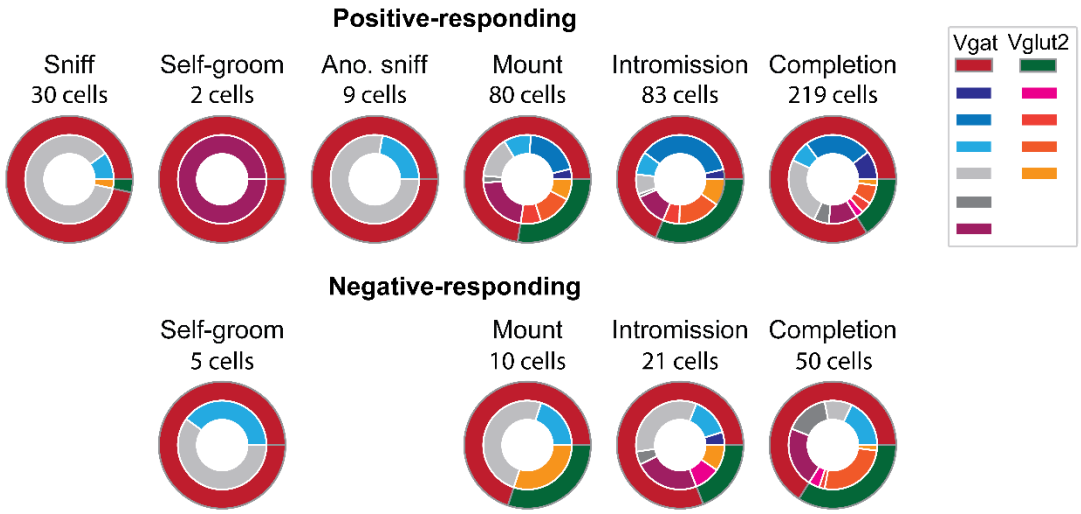

Figure S5: Distribution of subjects per cluster related to Figure 4.
Cells that had significant positive or negative response (>2δ) to each behavior onset were categorized as positive- or negative-responding cells respectively. Outer ring indicates the mouse line Vgat or Vglut2. The inner ring indicates each subject.

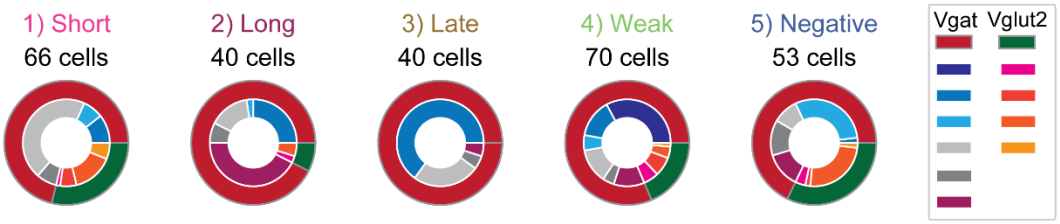

Figure S6: Distribution of subjects per cluster related to Figure 5.
Cells that had significant positive or negative response (>2δ) to each behavior onset were categorized as positive- or negative-responding cells respectively. Outer ring indicates the mouse line Vgat or Vglut2. The inner ring indicates each subject.

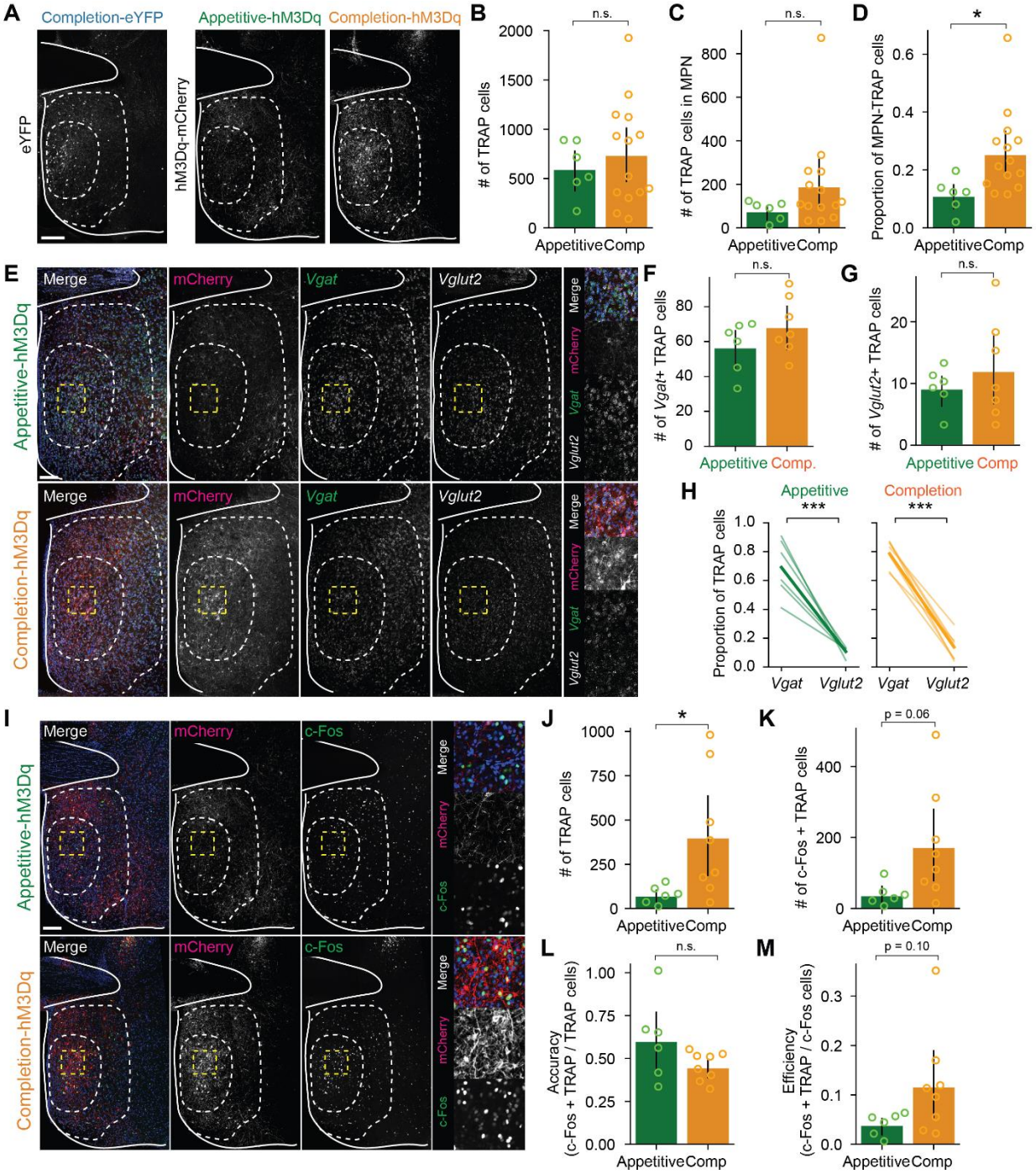

Figure S7: Histological analysis of TRAP labeling related to Figure 6.
(**A**) Histological analysis of the distribution of TRAP labeled cells. Representative coronal section showing eYFP or hM3Dq-mCherry expression in the MPOA. Scale bar, 100 μm.
(**B–D**) Number of TRAP labeled cells (**B**), number of TRAP labeled cells in the MPN (**C**) and the proportion of cells in the MPN among all the cells (**D**). Data from Completion-eYFP and Completion-hM3Dq were grouped into Completion group. Appetitive group, n = 7. Completion group, n = 14.

(**E**) *In situ* RNA hybridization analysis of the excitatory and inhibitory marker gene expression in the MPN. Appetitive-hM3Dq and Completion-hM3Dq groups were used for analysis. Representative coronal section showing mCherry, *Vgat* and *Vglut2* expression in the MPOA. Enlarged image indicated by the yellow box, is shown on the right.

(**F–H**) Number of *Vgat*+ TRAP labeled cells in the MPN (**F**), number of *Vglut2*+ TRAP labeled cells in the MPN (**G**) and the proportion of TRAP labeled cells that express *Vgat* or *Vglut2* (**H**). Appetitive group, n = 6. Completion group, n = 7.

(**I**) Antibody analysis of c-Fos expression after reactivation of mating completion ensemble. Representative coronal section showing mCherry and c-Fos expression in the MPOA. Enlarged image indicated by the yellow box, is shown on the right.

(**J–M**) Number of TRAP labeled cells in the MPN (**J**), number of c-Fos+ TRAP labeled cells in the MPN (**K**), the accuracy score (proportion of c-Fos+ TRAP labeled cells among all TRAP labeled cells) (**L**) and the efficiency score (proportion of c-Fos+ TRAP labeled cells among all c-Fos+ cells) (**M**). Appetitive group, n = 6. Completion group, n = 8.

All data are shown by thin lines for individual subjects and thick lines for mean. The data were analyzed by Student's t-test (**B, C, D, F, G, H, J, K, L, M**), Student's relative t-test with Bonferroni correction (**H**). $^{*}p < 0.05$, $^{**}p < 0.01$, $^{***}p < 0.001$; ns, not significant.

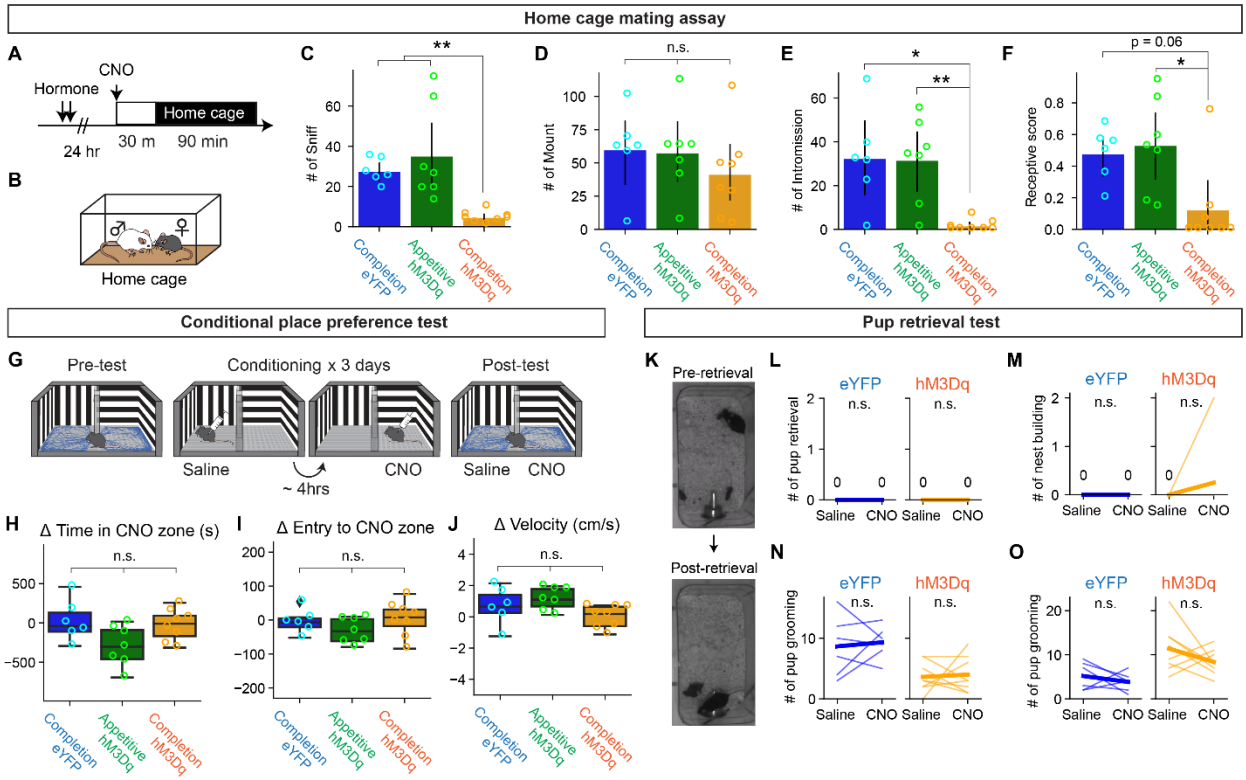

Figure S8: MPOA^{Completion} cells supress female sexual behavior in home cage mating assay but not other behaviors, related to Figure 6.

(**A**) Schematic of pharmaco-genetic activation of MPOA neurons during a home cage mating assay. Female subjects were primed with hormone before the experiment day. On the experiment day, subjects were injected i.p. with CNO to activate TRAP cells 30 minutes before the experiment. Animal behavior was recorded for 90 minutes.

(**B**) The male intruder was placed into the home cage of the female subject.

(**C–F**) Number of female-to-male sniff (**C**), male mounting (**D**), male intromission (**E**) and the receptive score (number of mounting episodes with intromissions over all mounting episodes).

(**G**) Schematic of conditional place preference (CPP) assay to evaluate the valence of activation of MPOA neurons. A two-chamber behavior apparatus, one room with vertical stripes and one room with horizontal stripes. On the first day animals were placed in the behavior apparatus to test their initial preference to each room for 30 minutes (Pre-test). On the conditioning days, the animals were placed in one side of the room where they were i.p. injected with either saline as control or CNO. CNO was injected 4 hours after the saline injection. On the last day, the animals were placed in the behavior apparatus to test their preference 30 minutes (Post-test).

(**H–J**) The difference in the time spent in the CNO zone (Time spent in the CNO zone in Post-test – Pre-test) (**H**), the difference in the number of CNO zone entries (Entries in Post-test – Pre-test) (**I**) and the difference in velocity of the animal (Velocity in Post-test – Pre-test) (**J**).

(**K**) Representative image of pup retrieval test. Female subject was i.p. injected with saline as control or CNO in their home cage. 30-minutes after injection, 3x 7w-old pup was placed in the corner of the home cage. Animal behavior was examined for 10 minutes.

(**L–O**) The number of pup retrievals (**L**), the number of nest building (**M**), the number of pup grooming (**N**) and the number of pup sniffing (**O**).

All data are shown by thin lines for individual subjects and thick lines for mean. The data were analyzed by Mann–Whitney U test with Bonferroni correction (**C–F**, **H–J**) and Wilcoxon rank sum

test (**L–O**) with Bonferroni correction. Completion-eYFP: n = 6, Appetitive-hM3Dq: n = 7, Completion-hM3Dq: n = 8. $^{*}p < 0.05$, $^{**}p < 0.01$, $^{***}p < 0.001$; ns, not significant.

Statistical analysis:

Table 1:

p-values were adjusted for post-hoc test/multiple comparison.

Figure	Test	Comparison	p-value
1H	two-way RM ANOVA	NA	0.00
1H	Tukey HSD post-hoc test	Control vs. Pre	0.63
1H	Tukey HSD post-hoc test	Control vs. Post	0.00
1H	Tukey HSD post-hoc test	Pre vs. Post	0.01
1I	two-way RM ANOVA	NA	0.00
1I	Tukey HSD post-hoc test	Control vs. Post	0.00
1I	Tukey HSD post-hoc test	Control vs. Pre	0.54
1I	Tukey HSD post-hoc test	Pre vs. Post	0.01
1J	Wilcoxon signed-rank test	Pre vs. Post	0.65
1K	Wilcoxon signed-rank test	Pre vs. Post	0.00
1L	Wilcoxon signed-rank test	Pre vs. Post	0.00
1M	Wilcoxon signed-rank test	Pre vs. Post	0.03
3H	Student’s t-test with Bonferroni correction	Sniff	0.00
3H	Student’s t-test with Bonferroni correction	Self-groom	0.00
3H	Student’s t-test with Bonferroni correction	Ano. Sniff	0.00

3H	Student’s t-test with Bonferroni correction	Mount	1.00
3H	Student’s t-test with Bonferroni correction	Intromission	1.00
3H	Student’s t-test with Bonferroni correction	Completion	0.00
3I	chisquare test with Bonferroni correction	Sniff, positive	0.00
3I	chisquare test with Bonferroni correction	Self-groom, positive	0.17
3I	chisquare test with Bonferroni correction	Ano. Sniff, positive	0.89
3I	chisquare test with Bonferroni correction	Mount, positive	0.71
3I	chisquare test with Bonferroni correction	Intromission, positive	0.99
3I	chisquare test with Bonferroni correction	Completion, positive	0.00
3I	chisquare test with Bonferroni correction	Sniff, negative	NA
3I	chisquare test with Bonferroni correction	Self-groom, negative	NA
3I	chisquare test with Bonferroni correction	Ano. Sniff, negative	0.49
3I	chisquare test with Bonferroni correction	Mount, negative	1.00
3I	chisquare test with Bonferroni correction	Intromission, negative	0.59
3I	chisquare test with Bonferroni correction	Completion, negative	1.00
4C	Student’s t-test with Bonferroni correction	Sniff: Sniff cell vs. Mount cell	0.00
4C	Student’s t-test with Bonferroni correction	Sniff: Completion cell vs. Mount cell	1.00
4C	Student’s t-test with Bonferroni correction	Sniff: Sniff cell vs. Completion cell	0.00

4C	Student’s t-test with Bonferroni correction	Self-groom: Sniff cell vs. Mount cell	1.00
4C	Student’s t-test with Bonferroni correction	Self-groom: Completion cell vs. Mount cell	1.00
4C	Student’s t-test with Bonferroni correction	Self-groom: Sniff cell vs. Completion cell	1.00
4C	Student’s t-test with Bonferroni correction	Ano. sniff: Sniff cell vs. Mount cell	0.04
4C	Student’s t-test with Bonferroni correction	Ano. sniff: Completion cell vs. Mount cell	0.00
4C	Student’s t-test with Bonferroni correction	Ano. sniff: Sniff cell vs. Completion cell	1.00
4C	Student’s t-test with Bonferroni correction	Mount: Sniff cell vs. Mount cell	0.00
4C	Student’s t-test with Bonferroni correction	Mount: Completion cell vs. Mount cell	0.00
4C	Student’s t-test with Bonferroni correction	Mount: Sniff cell vs. Completion cell	0.98
4C	Student’s t-test with Bonferroni correction	Intromission: Sniff cell vs. Mount cell	0.13
4C	Student’s t-test with Bonferroni correction	Intromission: Completion cell vs. Mount cell	0.00
4C	Student’s t-test with Bonferroni correction	Intromission: Sniff cell vs. Completion cell	0.15
4C	Student’s t-test with Bonferroni correction	Completion: Sniff cell vs. Mount cell	0.21
4C	Student’s t-test with Bonferroni correction	Completion: Completion cell vs. Mount cell	0.00
4C	Student’s t-test with Bonferroni correction	Completion: Sniff cell vs. Completion cell	0.00
5C	Student’s t-test	Vgat vs. Vglut2	0.00
5G	two-way ANOVA	NA	0.00
5G	Tukey HSD post-hoc test	Cluster 1 vs. Cluster 2	0.90

5G	Tukey HSD post-hoc test	Cluster 1 vs. Cluster 3	0.00
5G	Tukey HSD post-hoc test	Cluster 1 vs. Cluster 4	0.32
5G	Tukey HSD post-hoc test	Cluster 1 vs. Cluster 5	0.01
5G	Tukey HSD post-hoc test	Cluster 2 vs. Cluster 3	0.00
5G	Tukey HSD post-hoc test	Cluster 2 vs. Cluster 4	0.70
5G	Tukey HSD post-hoc test	Cluster 2 vs. Cluster 5	0.00
5G	Tukey HSD post-hoc test	Cluster 3 vs. Cluster 4	0.00
5G	Tukey HSD post-hoc test	Cluster 3 vs. Cluster 5	0.00
5G	Tukey HSD post-hoc test	Cluster 4 vs. Cluster 5	0.00
5G	two-way ANOVA	NA	0.00
5G	Tukey HSD post-hoc test	Cluster 1 vs. Cluster 2	0.00
5G	Tukey HSD post-hoc test	Cluster 1 vs. Cluster 3	0.00
5G	Tukey HSD post-hoc test	Cluster 1 vs. Cluster 4	0.00
5G	Tukey HSD post-hoc test	Cluster 1 vs. Cluster 5	0.00
5G	Tukey HSD post-hoc test	Cluster 2 vs. Cluster 3	0.65
5G	Tukey HSD post-hoc test	Cluster 2 vs. Cluster 4	0.00
5G	Tukey HSD post-hoc test	Cluster 2 vs. Cluster 5	0.56
5G	Tukey HSD post-hoc test	Cluster 3 vs. Cluster 4	0.10

5G	Tukey HSD post-hoc test	Cluster 3 vs. Cluster 5	0.90
5G	Tukey HSD post-hoc test	Cluster 4 vs. Cluster 5	0.09
5K	chisquare test with Bonferroni correction	Cluster 1: Vgat vs. Vglut2	0.00
5K	chisquare test with Bonferroni correction	Cluster 2: Vgat vs. Vglut2	0.12
5K	chisquare test with Bonferroni correction	Cluster 3: Vgat vs. Vglut2	0.02
5K	chisquare test with Bonferroni correction	Cluster 4: Vgat vs. Vglut2	0.79
5K	chisquare test with Bonferroni correction	Cluster 5: Vgat vs. Vglut2	1.00
6F	Wilcoxon signed-rank test with Bonferroni correction	Completion-hM3Dq: Saline vs. CNO	0.02
6F	Wilcoxon signed-rank test with Bonferroni correction	Completion-eYFP: Saline vs. CNO	1.00
6F	Wilcoxon signed-rank test with Bonferroni correction	Appetitive-hM3Dq: Saline vs. CNO	0.66
6G	Wilcoxon signed-rank test with Bonferroni correction	Completion-hM3Dq: Saline vs. CNO	0.02
6G	Wilcoxon signed-rank test with Bonferroni correction	Completion-eYFP: Saline vs. CNO	0.9375
6G	Wilcoxon signed-rank test with Bonferroni correction	Appetitive-hM3Dq: Saline vs. CNO	0.66
6H	Wilcoxon signed-rank test with Bonferroni correction	Completion-hM3Dq: Saline vs. CNO	0.08
6H	Wilcoxon signed-rank test with Bonferroni correction	Completion-eYFP: Saline vs. CNO	0.28125
6H	Wilcoxon signed-rank test with Bonferroni correction	Appetitive-hM3Dq: Saline vs. CNO	1.00
6I	Wilcoxon signed-rank test with Bonferroni correction	Completion-hM3Dq: Saline vs. CNO	0.05
6I	Wilcoxon signed-rank test with Bonferroni correction	Completion-eYFP: Saline vs. CNO	1.00

6I	Wilcoxon signed-rank test with Bonferroni correction	Appetitive-hM3Dq: Saline vs. CNO	0.89
6J	Wilcoxon signed-rank test with Bonferroni correction	Completion-hM3Dq: Saline vs. CNO	0.05
6J	Wilcoxon signed-rank test with Bonferroni correction	Completion-eYFP: Saline vs. CNO	0.65625
6J	Wilcoxon signed-rank test with Bonferroni correction	Appetitive-hM3Dq: Saline vs. CNO	1.00
6K	Wilcoxon signed-rank test with Bonferroni correction	Completion-hM3Dq: Saline vs. CNO	0.02
6K	Wilcoxon signed-rank test with Bonferroni correction	Completion-eYFP: Saline vs. CNO	0.46875
6K	Wilcoxon signed-rank test with Bonferroni correction	Appetitive-hM3Dq: Saline vs. CNO	1.00
6L	Wilcoxon signed-rank test with Bonferroni correction	Completion-hM3Dq: Saline vs. CNO	0.02
6L	Wilcoxon signed-rank test with Bonferroni correction	Completion-eYFP: Saline vs. CNO	0.9375
6L	Wilcoxon signed-rank test with Bonferroni correction	Appetitive-hM3Dq: Saline vs. CNO	0.47
S1A	Mann-Whitney U test	Virgin vs. SE	0.04
S1B	Mann-Whitney U test	Virgin vs. SE	0.03
S3D	Student’s t-test with Bonferroni correction	MPN: Appetitive vs. Completion	0.01
S3D	Student’s t-test with Bonferroni correction	MPA: Appetitive vs. Completion	0.51
S3D	Student’s t-test with Bonferroni correction	BNST: Appetitive vs. Completion	1.00
S3D	Student’s t-test with Bonferroni correction	LPO: Appetitive vs. Completion	1.00
S3D	Student’s t-test with Bonferroni correction	vLPO: Appetitive vs. Completion	1.00
S3I	Student’s t-test with Bonferroni correction	Vglut2: Appetitive vs. Completion	0.02
S3I	Student’s t-test with Bonferroni correction	Vgat: Appetitive vs. Completion	0.02

S3J	Student’s t-test with Bonferroni correction	Vgat-Calcr: Appetitive vs. Completion	0.03
S3J	Student’s t-test with Bonferroni correction	Vgat-Esr1: Appetitive vs. Completion	0.07
S3J	Student’s t-test with Bonferroni correction	Vgat-Gal: Appetitive vs. Completion	0.02
S3J	Student’s t-test with Bonferroni correction	Vgat-Nts: Appetitive vs. Completion	0.15
S3J	Student’s t-test with Bonferroni correction	Vgat-Prlr: Appetitive vs. Completion	0.02
S3J	Student’s t-test with Bonferroni correction	Vglut2-Calcr: Appetitive vs. Completion	0.01
S3J	Student’s t-test with Bonferroni correction	Vglut2-Esr1: Appetitive vs. Completion	0.82
S3J	Student’s t-test with Bonferroni correction	Vglut2-Gal: Appetitive vs. Completion	0.13
S3J	Student’s t-test with Bonferroni correction	Vglut2-Nts: Appetitive vs. Completion	0.20
S3J	Student’s t-test with Bonferroni correction	Vglut2-Prlr: Appetitive vs. Completion	0.10
S3M	Student’s t-test with Bonferroni correction	Cluster 1: Appetitive vs. Completion	0.02
S3M	Student’s t-test with Bonferroni correction	Cluster 2: Appetitive vs. Completion	0.00
S3M	Student’s t-test with Bonferroni correction	Cluster 3: Appetitive vs. Completion	0.03
S3M	Student’s t-test with Bonferroni correction	Cluster 4: Appetitive vs. Completion	1.00
S3M	Student’s t-test with Bonferroni correction	Cluster 5: Appetitive vs. Completion	0.38
S3M	Student’s t-test with Bonferroni correction	Cluster 6: Appetitive vs. Completion	0.63
S7B	Student’s t-test	Appetitive vs. Completion	0.03059692
S7C	Student’s t-test	Appetitive vs. Completion	0.21750181
S7D	Student’s t-test	Appetitive vs. Completion	0.03059692

S7F	Student's t-test	Appetitive vs. Completion	0.21047443
S7G	Student's t-test	Appetitive vs. Completion	0.44527542
S7H	Student's relative t-test	*Vgat*+ vs. *Vglut2*+	0.00118757
S7H	Student's relative t-test	*Vgat*+ vs. *Vglut2*+	8.47E-06
S7J	Student's t-test	Appetitive vs. Completion	0.04427996
S7K	Student's t-test	Appetitive vs. Completion	0.05979586
S7L	Student's t-test	Appetitive vs. Completion	0.11258612
S7M	Student's t-test	Appetitive vs. Completion	0.10375803
S8C	Mann-Whitney U test with Bonferroni correction	Completion-eYFP vs. Appetitive-hM3Dq	1
S8C	Mann-Whitney U test with Bonferroni correction	Completion-eYFP vs. Completion-hM3Dq	0.00716417
S8C	Mann-Whitney U test with Bonferroni correction	Appetitive-hM3Dq vs. Completion-hM3Dq	0.00429477
S8D	Mann-Whitney U test with Bonferroni correction	Completion-eYFP vs. Appetitive-hM3Dq	1
S8D	Mann-Whitney U test with Bonferroni correction	Completion-eYFP vs. Completion-hM3Dq	0.41161698
S8D	Mann-Whitney U test with Bonferroni correction	Appetitive-hM3Dq vs. Completion-hM3Dq	0.48907315
S8E	Mann-Whitney U test with Bonferroni correction	Completion-eYFP vs. Appetitive-hM3Dq	1
S8E	Mann-Whitney U test with Bonferroni correction	Completion-eYFP vs. Completion-hM3Dq	0.01651452
S8E	Mann-Whitney U test with Bonferroni correction	Appetitive-hM3Dq vs. Completion-hM3Dq	0.00956381
S8F	Mann-Whitney U test with Bonferroni correction	Completion-eYFP vs. Appetitive-hM3Dq	1
S8F	Mann-Whitney U test with Bonferroni correction	Completion-eYFP vs. Completion-hM3Dq	0.062566
S8F	Mann-Whitney U test with Bonferroni correction	Appetitive-hM3Dq vs. Completion-hM3Dq	0.02836664
S8H	Mann-Whitney U test with Bonferroni correction	Completion-eYFP vs. Appetitive-hM3Dq	0.22027972
S8H	Mann-Whitney U test with Bonferroni correction	Completion-eYFP vs. Completion-hM3Dq	1
S8H	Mann-Whitney U test with Bonferroni correction	Appetitive-hM3Dq vs. Completion-hM3Dq	0.16223776
S8I	Mann-Whitney U test with Bonferroni correction	Completion-eYFP vs. Appetitive-hM3Dq	1.00
S8I	Mann-Whitney U test with Bonferroni correction	Completion-eYFP vs. Completion-hM3Dq	1.00
S8I	Mann-Whitney U test with Bonferroni correction	Appetitive-hM3Dq vs. Completion-hM3Dq	0.6955711
S8J	Mann-Whitney U test with Bonferroni correction	Completion-eYFP vs. Appetitive-hM3Dq	1.00
S8J	Mann-Whitney U test with Bonferroni correction	Completion-eYFP vs. Completion-hM3Dq	0.84715285

S8J	Mann-Whitney U test with Bonferroni correction	Appetitive-hM3Dq vs. Completion-hM3Dq	0.06153846
S8L	Wilcoxon signed-rank test with Bonferroni correction	Completion-eYFP: Saline vs. CNO	1.00
S8L	Wilcoxon signed-rank test with Bonferroni correction	Completion-hM3Dq: Saline vs. CNO	1.00
S8M	Wilcoxon signed-rank test with Bonferroni correction	Completion-eYFP: Saline vs. CNO	1.00
S8M	Wilcoxon signed-rank test with Bonferroni correction	Completion-hM3Dq: Saline vs. CNO	0.63462102
S8N	Wilcoxon signed-rank test with Bonferroni correction	Completion-eYFP: Saline vs. CNO	1.00
S8N	Wilcoxon signed-rank test with Bonferroni correction	Completion-hM3Dq: Saline vs. CNO	1.00
S8O	Wilcoxon signed-rank test with Bonferroni correction	Completion-eYFP: Saline vs. CNO	1.00
S8O	Wilcoxon signed-rank test with Bonferroni correction	Completion-hM3Dq: Saline vs. CNO	0.390625

Table 2:
Related to **Figure 2C**. Student's t-test with Benjamini/Hochberg correction (FDR = 0.05).

name	acronym	pvalues	tvalues	qvalues
Striatum	STR	0.027581	2.77285	0.045968
Pallidum	PAL	0.015893	3.161613	0.045968
Thalamus	TH	0.017263	3.102443	0.045968
Hypothalamus	HY	0.021564	2.944859	0.045968
Midbrain, motor related	MBmot	0.02452	2.854778	0.045968
Pons	P	0.017438	3.095273	0.045968
Cortical plate	CTXpl	0.053019	2.32479	0.053019
Cortical subplate	CTXsp	0.047561	2.398637	0.053019
Midbrain, sensory related	MBsen	0.051409	2.345741	0.053019
Midbrain, behavioral state related	MBsta	0.05056	2.357055	0.053019

Table 3:
Related to **Figure 2I**. Student's t-test with Benjamini/Hochberg correction (FDR = 0.10).

name	acronym	pvalues	tvalues	qvalues	delta_density
Retroethmoid nucleus	REth	0.00027035	6.728201396	0.048933416	214984.2271
Paraventricular hypothalamic nucleus, anterior part	PVH	0.033005769	2.648661283	0.094438095	1511029.412
Paraventricular hypothalamic nucleus, descending division	PVHd	0.010790015	3.443218231	0.094438095	1237320.574
Pontine nuclei	Pn	0.01399666	3.253126975	0.094438095	726364.2458
Medial preoptic nucleus	MPN	0.025213586	2.83530796	0.094438095	538418.8992
Arcuate hypothalamic nucleus	Arc	0.024835753	2.84584565	0.094438095	471276.0549
Subincertal nucleus	SubI	0.038885676	2.536085916	0.094438095	456159.4203
Basomedial amygdaloid nucleus, anterior part	BMA	0.032450419	2.660354911	0.094438095	420379.5202
Dorsomedial hypothalamic nucleus	DM	0.019515865	3.015284468	0.094438095	417722.4199
Anterior olfactory area	AO	0.033850867	2.631254047	0.094438095	396076.7341
Medial amygdaloid nucleus	MeA	0.034215497	2.623882648	0.094438095	393432.2465
Geniculate group, ventral thalamus	GENv	0.010980212	3.430335334	0.094438095	392517.9631
Parastrial nucleus	PS	0.023075176	2.897283339	0.094438095	389577.7179
Posterior hypothalamic area	PHA	0.007812717	3.684538359	0.094438095	344105.2824
Dorsal hypothalamic area	DA	0.031337287	2.684434844	0.094438095	328994.4479
Cingulate cortex, area 29 and 30 (retrosplenial cortex)	A29-30 (RS)	0.041994152	2.483502759	0.094438095	328607.5648
Septohypothalamic nucleus	SHy	0.028271248	2.755685637	0.094438095	308183.0791
Intercalated nuclei of the amygdala	I	0.022153649	2.925884494	0.094438095	303098.2591
Medial preoptic area	MPA	0.024234861	2.86295712	0.094438095	293455.4286
Visual cortex	V	0.040142703	2.514316814	0.094438095	288986.0154
Bed nuclei of the stria terminalis	BNST	0.014648417	3.220245635	0.094438095	276911.809
Ventral claustrum	VCl	0.043305867	2.462507491	0.094438095	273015.1549
Retrocommissural nucleus	ReC	0.007195956	3.747046661	0.094438095	272060.6827
Posterodorsal preoptic nucleus	PDPO	0.022789588	2.906016112	0.094438095	256521.7391
Posterior intralaminar thalamic nucleus	PIL	0.006270716	3.852670343	0.094438095	254673.4955
Anterior hypothalamic nucleus	AHN	0.031414233	2.682741807	0.094438095	245409.5705
Midline group of the dorsal thalamus	MTN	0.041053196	2.498984166	0.094438095	245174.9444

Lateral hypothalamic area	LH	0.026869085	2.791014881	0.094438095	240716.549
Central amygdalar nucleus	Ce	0.02295482	2.900949615	0.094438095	222756.7068
Reticulotegmental nucleus of the pons	RtTg	0.039861128	2.519131285	0.094438095	220716.7925
Dorsal raphÃˆ nucleus	DR	0.037131527	2.567712711	0.094438095	215809.7069
Mammillary body	MBO	0.017042067	3.111637912	0.094438095	213150.9899
Parabrachial nucleus	PB	0.029873504	2.717496205	0.094438095	210519.415
Nucleus of the lateral olfactory tract	LOT	0.032785092	2.653283207	0.094438095	209776.8576
Lateral septal nucleus	LS	0.012997823	3.306843539	0.094438095	199090.867
Ventrolateral periaqueductal gray	VLPAG	0.021543468	2.9455231	0.094438095	198818.392
cortical amygdaloid nucleus	CoA	0.036772994	2.574367261	0.094438095	192850.1163
Perifornical nucleus	PeF	0.042635974	2.473146689	0.094438095	190273.5562
Ectorhinal cortex	Ect	0.037400229	2.562768988	0.094438095	183903.725
Retrochiasmatic area	RCh	0.022093224	2.927803596	0.094438095	183412.0027
Piriform cortex	PIR	0.042270032	2.479031476	0.094438095	179410.0145
Peripeduncular nucleus	PP	0.025025975	2.840519457	0.094438095	178242.6778
Subbrachial nucleus	SubB	0.039880447	2.518799838	0.094438095	176055.7372
Supratrigeminal nucleus	Su5	0.043119463	2.465450836	0.094438095	172176.5601
Basolateral amygdaloid nucleus, anterior part	BLA	0.027238194	2.781530404	0.094438095	170925.9594
Zona incerta	ZI	0.019402799	3.019398151	0.094438095	170116.803
Amygdalohippocampal area, anterolateral part	AHiAL	0.043006145	2.467246564	0.094438095	168524.9003
Basomedial amygdaloid nucleus, posterior part	BMP	0.042059695	2.48243775	0.094438095	163950.1212
Taenia tecta	TT	0.013837948	3.261382452	0.094438095	163679.9824
Lateral preoptic area	LPO	0.014148933	3.245300129	0.094438095	163257.4638
Cingulate cortex, area 25 (dorsal peduncular cortex)	A25 (DP)	0.022614385	2.911430898	0.094438095	158901.0119
Retroendopiriform nucleus	REn	0.015140653	3.19643327	0.094438095	153821.656
Medial paralemniscial nucleus	MPL	0.024141756	2.865648399	0.094438095	152012.2652
Retrohippocampal region	RHP	0.020278105	2.988194957	0.094438095	147871.0864
Extension of the amygdala	EA	0.023167095	2.894496846	0.094438095	146421.754
Intralaminar nuclei of the dorsal thalamus	ILM	0.026268004	2.8067567	0.094438095	138466.3028
Accumbens nucleus	Acb	0.026656815	2.796531442	0.094438095	121049.4763
Anterior group of the dorsal thalamus	ATN	0.024872564	2.844811608	0.094438095	116513.7776

Medial septal complex	MSC	0.009287168	3.554533411	0.094438095	116015.1086
Basolateral amygdaloid nucleus, ventral part	BLV	0.034166225	2.624873956	0.094438095	111714.3319
Precuneiform area	PrCnF	0.03108891	2.689929629	0.094438095	111331.5111
Ventral linear nucleus of the thalamus	VLi	0.023533863	2.883493451	0.094438095	104255.3191
Granular insular cortex	GI	0.04004456	2.515990923	0.094438095	102452.5469
Medial group of the dorsal thalamus	MED	0.036719338	2.575368924	0.094438095	102189.3029
Trochlear nucleus shell region	4Sh	0.037350621	2.563678927	0.094438095	100890.2077
Perihinal cortex	PRh	0.02438704	2.858581625	0.094438095	100545.5575
Olfactory tubercle	Tu	0.029822837	2.718670704	0.094438095	99478.85791
Amygdalopiriform transition area	Apir	0.020731195	2.972599247	0.094438095	98027.60237
Basolateral amygdaloid nucleus, posterior part	BLP	0.029813416	2.718889311	0.094438095	96992.57798
Perilemniscal nucleus, ventral part	PLV	0.021951965	2.932311732	0.094438095	87094.63931
Retrorubral field	RRF	0.015997937	3.156872141	0.094438095	80496.68164
Rostral amygdalopiriform area	RAPir	0.02437059	2.859053227	0.094438095	80421.05263
Interstitial nucleus of the posterior limb of the anterior commissure	IPAC	0.04224291	2.479469719	0.094438095	74942.11667
Substantia innominata, basal part	SIB	0.007425637	3.723111671	0.094438095	73068.14478
Nucleus of the optic tract	OT	0.033877347	2.63071595	0.094438095	69853.21792
Lateral group of the dorsal thalamus	LAT	0.016271392	3.144727567	0.094438095	56321.48138
Ventral tegmental area, rostral part	VTAR	0.026117796	2.810749617	0.094438095	52016.77961
Hippocampal region	HIP	0.013705887	3.268329396	0.094438095	49111.41071
Superior olivary complex	SOC	0.034434805	2.619488322	0.094438095	48835.91738
Peritrigeminal zone	P5	0.041287707	2.495091809	0.094438095	44322.79711
Motor trigeminal nucleus	5N	0.026671294	2.796153682	0.094438095	33511.87288
Red nucleus, parvicellular part	RPC	0.034054182	2.627133695	0.094438095	29776.83316
Red nucleus, magnocellular part	RMC	0.036813675	2.573608826	0.094438095	16358.20896
Anteroventral periventricular nucleus	AVPe	0.047633537	2.397604142	0.095500403	350817.942
Superior colliculus, sensory related	SCs	0.045014824	2.436114638	0.095500403	279549.035
Amygdalohippocampal area, posteromedial part	AHiPM	0.046271675	2.417352681	0.095500403	197042.8783
Paraterete nucleus	PTe	0.044712593	2.440706472	0.095500403	138562.0915
Lateral amygdaloid nucleus, ventrolateral part	LaVL	0.049069268	2.377400884	0.095500403	111890.4636

Dorsal column nuclei	DCN	0.048875761	2.380088348	0.095500403	105843.8012
Subcoeruleus nucleus, ventral part	SubCV	0.047229154	2.403407129	0.095500403	104463.8445
Dysgranular insular cortex	DI	0.046799894	2.409623069	0.095500403	91543.87141
Paralemniscal nucleus	PL	0.047171454	2.404239291	0.095500403	91281.24728
Triangular septal nucleus	TS	0.0489075	2.379646797	0.095500403	90951.94923
Temporal association cortex	TeA	0.053048485	2.32441387	0.096612039	230410.4523
Anterior amygdaloid area	AA	0.051959553	2.338500252	0.096612039	213370.2496
Ventrolateral preoptic nucleus	VLPO	0.054752263	2.302953845	0.096612039	193767.7054
Dorsal claustrum	DCl	0.054385429	2.307516395	0.096612039	184893.095
Dorsal endopiriform nucleus	DEn	0.05460878	2.304734718	0.096612039	168921.3894
Septohippocampal nucleus	SHi	0.054067088	2.311501228	0.096612039	138820.827
Principal sensory trigeminal nucleus	Pr5	0.050736197	2.354689007	0.096612039	118023.4335
Subpeduncular tegmental nucleus	SPTg	0.054978122	2.300160119	0.096612039	60783.36557
Septofimbrial nucleus	SFi	0.051439223	2.345337804	0.096612039	53951.0591
Frontal association cortex	FrA	0.05128933	2.347320591	0.096612039	41017.44617
Oculomotor nucleus, parvicellular part	3PC	0.059164829	2.250381322	0.099715285	178397.8398
Anterior pretectal nucleus	APT	0.058241816	2.261041923	0.099715285	97058.17135
Retroparafascicular nucleus	RPF	0.059498623	2.246567454	0.099715285	75162.54874
Interstitial nucleus of Cajal, shell region	InCSh	0.058667656	2.256102481	0.099715285	63126.33834
Substantia nigra, compact part, medial tier	SNCM	0.057680716	2.267606435	0.099715285	59030.83699
Lateral periaqueductal gray	LPAG	0.060288777	2.23762485	0.100112557	194562.1315
Amygdalohippocampal area, posterolateral	AHiPL	0.061133938	2.228189851	0.100470249	89309.87819
Substantia nigra, compact part, dorsal tier	SNCD	0.061614352	2.222885272	0.100470249	34238.12462
Cingulate cortex, area 24a (infralimbic)	A24a (IL)	0.064427335	2.192638537	0.10160567	313726.1239
Parasubthalamic nucleus	PSTh	0.066633447	2.169833141	0.10160567	218198.1443
Cingulate cortex, area 32 (Prelimbic cortex)	A32 (PrL)	0.070589728	2.130771553	0.10160567	186709.6396
Superior colliculus, motor related	SCm	0.07045698	2.132046279	0.10160567	180898.379
Vascular organ of the lamina terminalis	VOLT	0.064209957	2.194928008	0.10160567	132695.9847
Laterodorsal tegmental nucleus	LDT	0.066182237	2.174435105	0.10160567	128972.7583
Olivary pretectal nucleus	OPT	0.068420146	2.151912393	0.10160567	128625.7469
Perihypoglossal nuclei	PHY	0.067768535	2.158393137	0.10160567	108035.7143

Geniculate group of the thalamus	GENd	0.064582441	2.191009662	0.10160567	95963.7295
Parainterfascicular nucleus of the VTA	PIF	0.068692279	2.149224137	0.10160567	93618.80772
Ethmoid thalamic nucleus	Eth	0.070731019	2.12941743	0.10160567	74055.90976
Subcoeruleus nucleus, dorsal part	SubCD	0.067468902	2.161394204	0.10160567	73155.25876
Ventral group thalamic nucleus	VENT	0.068854486	2.147626852	0.10160567	65230.91499
Caudate Putamen	CP	0.068112675	2.154962668	0.10160567	50048.9282
Reticular nucleus (prethalamus)	Rt	0.069375305	2.14252361	0.10160567	36383.73788
Cochlear nuclei	CN	0.074112107	2.097794939	0.10166659	389522.8563
Medial tuberal nucleus	MTu	0.074143591	2.097507297	0.10166659	290098.2977
Nucleus of stria medullaris	SM	0.072349461	2.114096451	0.10166659	164601.7699
Lateral amygdaloid nucleus, dorsolateral part	LaDL	0.072690277	2.110913789	0.10166659	161829.1029
Lateral amygdaloid nucleus, ventromedial part	LaVM	0.071639711	2.120772692	0.10166659	113223.3326
Basal nucleus (Meynert)	B	0.074023062	2.098609133	0.10166659	61843.79002
parietal association cortex	PtA	0.075429427	2.085862405	0.102652078	300124.8439
Subthalamic nucleus	STh	0.076670914	2.074805206	0.103562952	96753.1352
Suprachiasmatic nucleus	SCh	0.078150136	2.061860784	0.10372961	536853.5655
Bed nucleus of the accessory olfactory tract	BAOT	0.078169219	2.061695393	0.10372961	250000
Agranular insular cortex	AI	0.078513572	2.05871767	0.10372961	78845.46255
prosomere 1 periaqueductal gray	p1PAG	0.080340941	2.043129639	0.105374712	118788.2106
motor cortex	M	0.081173862	2.036140829	0.105701216	130495.2704
Epithalamus	EPI	0.083627244	2.015960265	0.107463349	81692.56281
Parabranchial pigmented nucleus of the VTA	PBP	0.083714542	2.015253018	0.107463349	61538.46155
Dorsal tegmental nucleus	DTg	0.086064237	1.996485547	0.109701598	81452.07034
Premamillary nucleus, ventral part	PMV	0.086829218	1.990484411	0.109902717	529920.2128
Accessory supraoptic group	ASO	0.088800509	1.975256779	0.111238126	388571.4286
Ventromedidal preoptic nucleus	VMPO	0.090080505	1.965546231	0.111238126	338996.139
Pre-Edinger-Westphal nucleus	PrEW	0.089909997	1.966831915	0.111238126	280612.2449
Ventromedial hypothalamic nucleus	VMH	0.090359395	1.963448451	0.111238126	190331.0267
Subfornical organ	SFO	0.090957142	1.958973613	0.111238126	180695.6522
Cingulate cortex	A24 (Cg)	0.092690124	1.946161436	0.112065812	255749.0006
Medial pretectal area	MPT	0.09287222	1.944828831	0.112065812	169027.0582

Bed nucleus of the anterior commissure	BAC	0.096091042	1.921686027	0.114424202	160000
Pontine reticular nucleus	PRNr	0.095727904	1.924258672	0.114424202	47422.31481
Pleoglial periaqueductal gray	PlPAG	0.097604364	-1.911066172	0.115466601	-514285.7144
Auditory cortex	Au	0.099726102	1.89644406	0.116454352	262322.801
Somatosensory cortex	S	0.099168015	1.90026056	0.116454352	153428.4546
Orbital cortex	O	0.108138179	1.841302477	0.123907217	197537.6873
Periventricular hypothalamic nucleus	Pe	0.108846671	1.836849825	0.123907217	192549.7534
Commissural nucleus of the inferior colliculus	Com	0.108586478	1.838481793	0.123907217	192190.8894
Median preoptic nucleus	MnPO	0.10736765	1.846177138	0.123907217	176415.0943
Supraoptic nucleus	SO	0.112074861	1.81690943	0.125997204	378076.7314
Posterior pretectal nucleus	PPT	0.111938479	1.817740589	0.125997204	104522.6131
Subparafascicular thalamic nucleus	SPF	0.113499108	1.808287319	0.126810732	226977.1955
Ventral endopiriform nucleus	VEn	0.114552457	1.80197726	0.127202421	116214.0575
Paraventricular hypothalamic nucleus, ventral part	PaV	0.116535881	1.790245474	0.12861582	647682.1193
Cell bridges of the ventral striatum	CB	0.131039242	1.709845396	0.143746078	36716.79198
Intermediate endopiriform claustrum	IEn	0.135764526	1.685471493	0.147922142	212660.6265
Nucleus raphÃˆ	NR	0.13648065	1.681847717	0.147922142	83163.61168
Interfascicular nucleus	IF	0.158156212	1.579831943	0.170394491	131558.1854
Ambiguus nucleus	Amb	0.16326766	1.557680295	0.17486063	70544.09005
Nucleus of the posterior commissure	PCom	0.170627952	1.526879882	0.181668584	84941.56928
Pontine raphÃˆ nucleus	PnR	0.184495141	1.472013908	0.19528433	96858.63874
Dorsolateral periaqueductal gray	DLPAG	0.187632923	1.460120451	0.197450925	97607.89562
Subparaventricular zone of the hypothalamus	SPa	0.205664825	1.395051632	0.215175337	237155.2975
Premamillary nucleus, dorsal part	PMD	0.20790761	1.387318267	0.216271709	99999.99999
Scaphoid thalamic nucleus	Sc	0.213846915	1.36719048	0.221178809	83168.31684
Dorsomedial periaqueductal gray	DMPAG	0.29338436	1.135908477	0.301719143	112181.3031
Rostral linear nucleus (midbrain)	RLi	0.295062345	1.131631116	0.301730421	83319.29231
Paratrochlear nucleus	Pa4	0.333513525	1.038637147	0.339134539	19108.28025
Paranigral nucleus of the VTA	PN	0.342480073	1.018192459	0.346306666	42133.33335
Caudal linear nucleus of the raphÃˆ	CLi	0.397136068	0.901787447	0.39934238	47018.73936

Interpeduncular nucleus	IP	0.459943892	0.781817731	0.459943892	61668.54567

1261